ChemComm
Chemical Communications

Accepted Manuscript

This article can be cited before page numbers have been issued, to do this please use: K. Ma, J. Sun and L. Dou, *Chem. Commun.*, 2024, DOI: 10.1039/D4CC02299H.

ROYAL SOCIETY OF CHEMISTRY

rsc.li/chemcomm

View Article Online
DOI: 10.1039/D4CC02299H

No primary research results, software or code have been included and no new data were generated or analysed as part of this review.

View Article Online
DOI: 10.1039/D4CC02299H

ARTICLE

Advances and Challenges in Molecular Engineering of 2D/3D Perovskite Heterostructures

Received 00th January 20xx,
Accepted 00th January 20xx

DOI: 10.1039/x0xx00000x

Ke Ma,*[a,b] Jiaonan Sun [c,d] and Letian Dou *[b,e,f]

Organic-inorganic hybrid perovskite have been intensively studied in the past decades due to their outstanding performance in solar cells and other optoelectronic devices. Recently, the emergence of two-dimensional/three-dimensional (2D/3D) heterojunctions have enabled many solar cell devices with >25% power conversion efficiency, which was driven by the advances in our understanding of the structural and photophysical properties of the heterojunctions and our ability in controlling these properties through organic cation configuration in 2D perovskites. In this feature article, we discuss the fundamental understanding of structure characteristics and the carrier dynamics in 2D/3D heterojunctions and their impacting factors. We further elaborate the design strategies of molecular configuration of the organic cations to achieve thorough management of these properties. Finally, the recent advances of 2D/3D heterostructures in solar cells, light emitting devices and photodetectors are highlighted, which translate the fundamental understandings to the device applications, and also reveal the remaining challenges in ligand design for next generation of stable devices. Future development prospects and related challenges are also provided with wide perspective and insightful thoughts.

1. Introduction

The requirements for decarbonizing the energy generation systems have attracted immense research on developing advanced photovoltaic technologies that can deliver high power conversion efficiency (PCE) and maintain excellent stability. Since 2009, when the first metal halide perovskite photovoltaic device was reported by Miyasaka and co-workers,[1] it become one of the most promising new techniques nowadays, with the highest PCE reaching to 26.1%.[2–5] The perovskite solar cells (PSCs), with its intrinsic outstanding optoelectronic properties and ease of fabrication, exhibit great potential of approaching to the theoretical efficiency limit in both single junction and multi-junction solar cells.[6]

The most commonly used light absorbing material in PSCs is the three-dimensional (3D) perovskite polycrystal thin film. The 3D perovskite structure has a general formular of ABX_3, where A as the monovalent cation (methylammonium (MA^+), formamidinium (FA^+) or Cs^+, etc.), B as the divalent metal cation (Pb^{2+}, Sn^{2+}, etc.), and X as the halide anion (I^-, Br^-, Cl^-). Any of the A, B and X sites can be tuned toward different applications, but still follows the Goldschmidt tolerance factor to maintain the structure stability.[7] Due to the ionic nature of perovskite structure and the low-temperature synthetic method, it is prone to forming defects within and on the surface of the material, influencing the optoelectronic properties, and more importantly initiating the degradation.[8] As the crystal symmetry is broken at the surface of grain and the defect densities grow exponentially,[9] including some deep defects, strategies are explored to passivate surface and grain boundaries to reduce the defect densities, such as adding additives or dopants.[10,11]

Besides 3D perovskite, the low-dimensional perovskites, including two-dimensional (2D), one-dimensional (1D) and zero-dimensional (0D) perovskites, have also been intensively investigated, offering a wide range of opportunities for tailoring the crystallographic structures.[12,13] The most widely studied low-dimensional perovskite structure is 2D perovskite, a layered structure formed by one or multiple layers of inorganic octahedra being sandwiched by two layers of bulky organic cations (also called ligands in this article), as illustrated in Fig. 1a. The ligand is composed of ammonium anchors and functional tails, while the selection of the functional groups will determine the properties of 2D perovskites. This type of layered structure has exhibited outstanding chemical stability, in comparison with 3D perovskites, owing to the ion migration barriers and moisture/oxygen barriers induced by the organic ligands.[13,14] The optoelectronic properties of 2D perovskites are influenced by the quantum confinement, showing the enlarged bandgaps and tunable energy levels. The stability and tunable optoelectronic properties of 2D perovskites enables stable PSCs and color-tunable light emitting diode (LED) devices, respectively.[15–17] However, the quantum confinement effect and high exciton binding energy inhibit the generation of free carriers, the key component in photovoltaic

[a] Global Institute of Future Technology, Shanghai Jiao Tong University, Shanghai, 200240, China.
[b] Davidson School of Chemical Engineering, Purdue University; West Lafayette, IN 47907, USA.
[c] Department of Materials Science and Engineering, City University of Hong Kong, Kowloon, Hong Kong 999077, China.
[d] Hong Kong Institute for Clean Energy (HKICE), City University of Hong Kong, Kowloon, Hong Kong 999077, China.
[e] Department of Chemistry, Purdue University; West Lafayette, IN 47907, USA.
[f] Birck Nanotechnology Center, Purdue University; West Lafayette, IN 47907, USA
* Corresponding author. Email: dou10@purdue.edu; ke.ma@sjtu.edu.cn.
Electronic Supplementary Information (ESI) available: [details of any supplementary information available should be included here]. See DOI: 10.1039/x0xx00000x

View Article Online
DOI: 10.1039/D4CC02299H

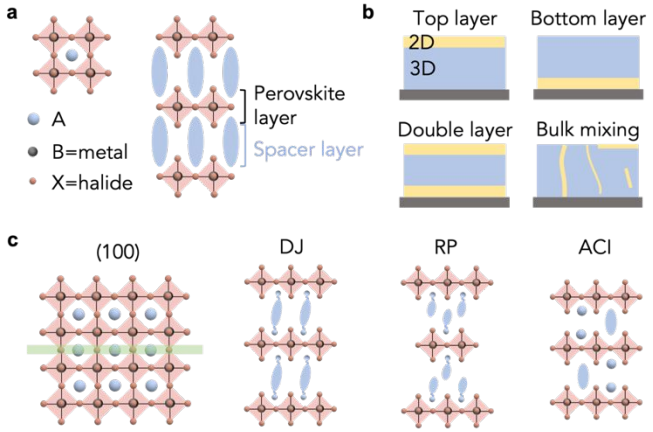

Fig. 1 (a) Crystal structure scheme of 3D perovskite and 2D perovskite. (b) Scheme of heterostructure types of 2D/3D perovskite thin films. (c) Scheme of different space groups and phases of 2D perovskites based on (100)-orientation.

devices. In addition, the bulky organic ligands suppress ion migration, but also induce barriers for charge transfer, which restricts the charge injection and collection in optoelectronic devices.

Different from pure 2D perovskites, the 2D/3D heterostructures combine the stability of 2D perovskites and the carrier dynamics advantages of 3D perovskites, emerging as a leading structure in optoelectronic devices. The layered heterojunction and bulk mixing are two major types of heterostructures (Fig. 1b), within which, the layered heterojunction has been widely explored due to its ordered structure, controlled fabrication process and excellent device performance.[18] The principle concept is forming 2D layers either on the surface or at the bottom of 3D perovskite grains (Fig. 1b), passivating the defects, and also protecting the surface from external environment. The most commonly used method for constructing the 2D/3D heterostructures in devices is by depositing ligand salt solution on to the as-synthesized 3D perovskite thin films and converting the surface of 3D perovskite into 2D perovskite in-situ. This type of cation exchange and structure conversion mechanism has also been demonstrated in the perovskite nanocrystals.[19] Based on this method, different strategies, including solvent engineering,[20–24] annealing engineering,[25,26] and processing engineering[27–29] have been developed to precisely manipulate the microstructures. Among them, for any given 2D perovskites, the ligand configuration is one of the most critical parameters that determines the structures, and subsequently the optoelectronic properties and long-term stability of the desired materials.

In this feature article, we undermine the performance-limiting characteristics in 2D/3D perovskite heterojunctions, and leverage the key roles of organic ligands in determining these characteristics. By examining the recent progress in understanding the structure and photophysical properties of 2D/3D heterojunctions, we build the structure-property-performance relationship to connect different aspects of previous research works on perovskite heterojunction, and generate design principles of the organic cation ligands. Meanwhile, we provide insights into the findings about the stability of 2D/3D heterojunctions in devices, and the ligand configurations on affecting the structure stability. Finally, we also present perspectives about the emerging directions to address the critical issues that have not been solved in the 2D/3D heterojunctions, specifically focusing on the ligand design.

2. Structural characteristics of 2D/3D heterojunction

The structural characteristics of 2D/3D perovskite heterojunctions can be grouped into two parts, the structure of 2D perovskites and the structure of 2D/3D heterojunctions. The description of the crystal structure of 2D perovskites encompasses the phase space, the thickness of the inorganic layers (or called perovskite layers), and the packing order of both inorganic octahedra and the organic cations, while that of 2D/3D heterostructure includes relative orientation and morphology. In this review article, the general chemical formula of 2D perovskite is written as $A'_2A_{n-1}B_nX_{3n+1}$, in which A' is the bulky organic ligand, and the n value is defined as the number of the octahedra layers that is sandwiched by the organic spacers along the stacking direction. We list the most widely studied ligands for the construction of 2D/3D heterojunction in Fig. 2, and will discuss the role of the molecular configurations of organic spacers in modulating the above-described structure characteristics.

2.1 Phase spaces

The phase spaces of 2D perovskites can be classified in three types, Ruddlesden-Popper (RP) phase, Dion Jacobson (DJ) phase, and alternating cation (ACI) phase (Fig.1c). The RP phase features the stacked perovskite layers shift by half a unit cell in the in-plane direction, while it can also be considered as being formed with mono-ammonium functional ligands (Fig. 2). In contrast, the DJ phase is formed with di-ammonium ligands (Fig. 2) and exhibits no in-plane shift between the stacked perovskite layer.[30] As described, the phase space of formed 2D perovskite is closely related with the number of ammonium functional groups on the spacer ligands. The mono-ammonium ligands in RP phase usually end with neutrally charged tail, which interacts with ligands in the neighboring layer through intermolecular forces. Van de Waals force or π interactions stem from aliphatic tails or aromatic tails, respectively, and the representative ligands are butylammonium (BA) or phenethylammonium (PEA). In contrast, the DJ phase 2D perovskite is composed of di-ammonium ligands, the interactions between neighboring organic layers are considered as covalent bonds. The notable differences in the out-of-plane and in-plane mechanical properties and structure stabilities between RP phase and DJ phase have been observed, attributed to the different interlayer interactions and stacking order.

The rigidity of ligands and the bonding types between the neighboring organic layers are two key factors that influence the structure and mechanical stability of 2D perovskites. The intra-molecular covalent bonds in DJ phase 2D perovskites are expected to be stronger than the intermolecular interactions in RP phase 2D structures. The flexible BA ligand in RP phase has been demonstrated to result in less distortion of octahedra in the in-plane direction, while the rigid 4-(aminomethyl)piperidinium (4AMP) ligand in DJ phase gave rise to greater distortion due to the stronger electrostatic interactions between the cyclic diammonium cation and the inorganic octahedra (Fig. 3a and 3b).[31] It has also been reported that

View Article Online
DOI: 10.1039/D4CC02299H

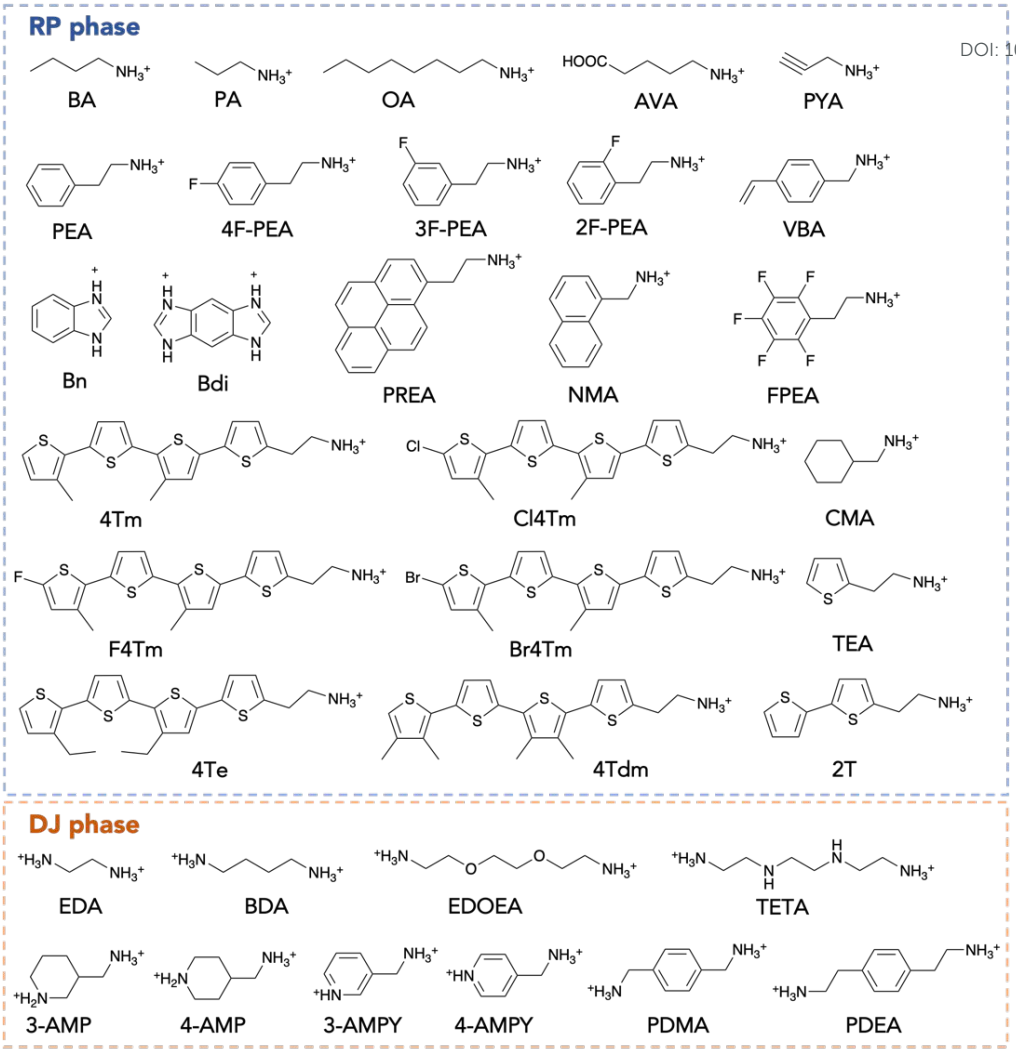

Fig. 2 Molecular structures of representative examples of organic cations used for 2D/3D heterojunction construction.

with similar rigidity, the benzimidazolium (Bn) cations, which forms RP phase 2D perovskite, only have weak intermolecular interactions to hold the structure together, while the divalent benzodiimidazolium (Bdi) cations shift the weakest link in 2D perovskite from intermolecular interactions to the bonds between cations and perovskite octahedra.[32] The RP and DJ phase 2D perovskites also exhibit significant differences in mechanical properties, including the Young's modulus.[33] Due to the thinner organic layer and more space portion of the rigid inorganic layer, DJ phase 2D perovskite exhibits increased moduli, and subsequently enhanced mechanical stability, comparing with RP phase structure.

Regarding the environmental stability, the 3D perovskites with 2D capping layers are usually considered with reduced moisture and oxygen penetration. In the case of RP phase 2D perovskites, the expected ending layer on surface is the tail of organic cations, which is neutrally charged and chemically stable. However, the surface ending group in DJ phase perovskite will be either the unbonded ammonium functional group or the perovskite octahedra layer, none of which is inert. The structure of DJ phase 2D perovskite can be disrupted in humid environment due to hydration, but the good news is that the original layered structure can be restored through annealing.[34] This analysis indicates that the environmental stability of 2D/3D heterostructures with DJ phase 2D perovskites is still a debatable problem. Therefore, although both RP phase and DJ phase structures have been used to create 2D/3D heterojunctions and been demonstrated with representative devices, there is no conclusion whether one type of structure has dominant advantages over the other, given various aspects of the two phases.

2.2 Thickness of inorganic perovskite layer

Another type of phase group in 2D perovskite is defined by the thickness of its perovskite layers. In this manuscript, we use the term "*n* phase" to refer to this type of phase group. The structure and physical properties of *n*=1 2D perovskites have seen intensive studies. However, limited understanding have gained in the thermodynamically stable 2D perovskite structures with *n*>1, also called quasi-2D perovskites, mainly due to the challenges of synthesizing phase-pure (narrow *n* value distribution) quasi-2D perovskite crystals.[35,36] Therefore, mostly studied growth methods of 2D/3D heterojunctions inevitably form a mixed phase quasi-2D perovskite layer atop of 3D perovskite thin films. Various state-of-the-art strategies have been developed to control the phase distribution of quasi-2D perovskites in both 2D structures and 2D/3D

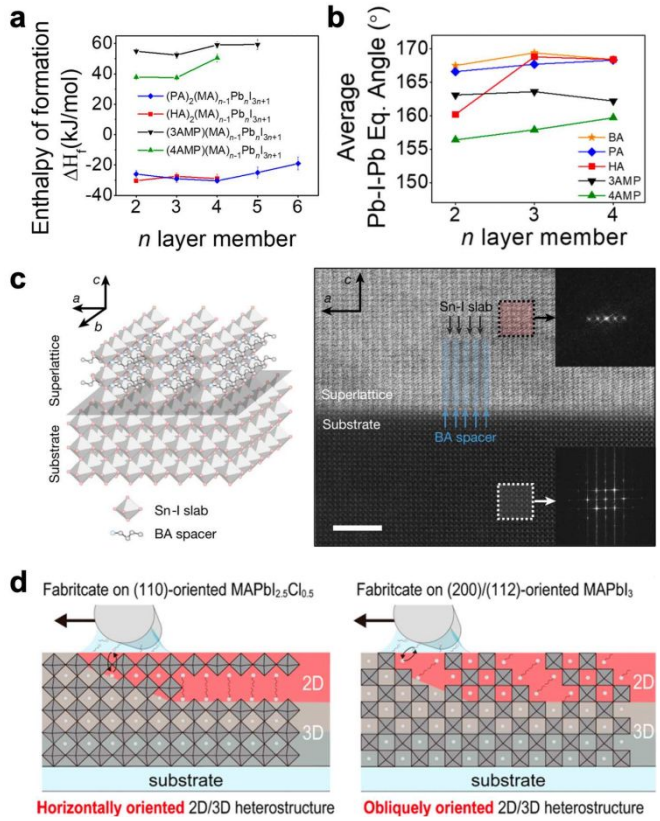

Fig. 3 (a-b) Enthalpy of formation (a) and Average equatorial Pb–I–Pb angle (b) for four different 2D perovskites as a function of perovskite layer thickness.[31] (c) Scheme (left) and atomic-resolution cryogenic STEM images (right) of $(BA)_2SnI_4$ vertically aligned on $MAPb_{0.5}Sn_{0.5}Br_3$ single crystal substrate.[46] (d) Scheme illustration of heterostructures fabricated on (110)-oriented $MAPbI_{2.5}Cl_{0.5}$ or (200)-/(112)-oriented $MAPbI_3$.[35]

heterostructures, such as solid-state growth,[27] annealing temperature control,[25] and solvent engineering,[24] beside which the molecular configurations of organic ligands are the deterministic characteristics of a thermodynamically stable 2D structure (Fig. 3a).

Chen et al. has demonstrated that the configuration of organic spacers can influence the phase purity and the preferred *n* values of the quasi-2D perovskite in 2D/3D heterojunction.[23] As bonding different ligands onto the quasi-2D perovskite flakes ($FA_{n-1}Pb_nI_{3n-1}$) will introduce different types of strains in the flakes due to the ligand packing geometry, perovskite lattice has to be distorted to release the strain. Mostly, bulkier organic ligand results in more lattice strain, and thicker perovskite flakes are required to fully release the strain, thus larger *n* value is preferred. The intermolecular interactions between neighboring organic ligands, like hydrogen bonds, could also cause octahedra distortion in the inorganic layers, which subsequently modulate the *n* values.[37–39] The same principle also applies to DJ phase 2D/3D heterojunction formed with 2,2-(ethylenedioxy)bis(ethylammonium) (EDOEA), that the suitable binding energy and hydrogen bonds between organic ligands and perovskite octahedra leads to the formation of phase pure *n*=1 structure, instead of mixed phases.[40] Beside determining the *n* phases through structure stability, the hydrogen bonding between cations like dimethyl adipimidate can induce uniformly distributed colloidal sizes in precursor solution, and result in spontaneously formed phase-pure 2D perovskite at the bottom of 3D perovskite thin films.[41] The other factor that influences the *n* values in 2D/3D heterojunction is the lattice matching between 2D and 3D structures.[42] The large lattice mismatching caused by the halide and cation differences in 2D and 3D perovskites results in lattice strain at interfaces, which facilitates the maintenance of pre-crystalized *n*=1 2D crystal in its original phase while incorporated into the 3D perovskite matrix, as phase transformation is less favorable. Based on this principle, the design of organic ligands can also play the role of generating large lattice mismatching between 2D and 3D perovskites, to stabilize the *n* phases. For example, the conjugated ligands offer various tunability on the molecular configurations to tune the lattice structures, such as heteroatom, conjugation length, and molecular twist (planarity), significantly suppressed the halide segregation and *n* phase separation, which requires more investigation and applications on 2D/3D heterojunctions.[43–45]

2.3 Orientation of 2D perovskites

Due to the anisotropic structure and electronic properties, the orientation of 2D perovskite in the devices is critical in determining the carrier dynamics. The orientation of 2D perovskites in heterojunctions can be grouped in three categories, vertical aligned, parallel aligned, and random oriented, with respect to the bottom 3D perovskite substrates. Most of 2D passivation layers in the state-of-the-art PSCs are parallel aligned with 3D perovskites, as reported by the X-ray diffraction (XRD) and Grazing incidence wide angle X-ray scattering (GIWAXS) patterns, due to the shallow ligand diffusion depth and the easy formation of parallel 2D perovskites on commonly used substrates.[24,25] However, by slowing down the crystal growth rate, Lei et al demonstrated heteroepitaxial growth of $BA_2MA_{n-1}Sn_nI_{3n+1}$ 2D crystal on $MAPb_{0.5}Sn_{0.5}Br_3$ 3D perovskite single crystal, which exhibited vertically oriented 2D structure (Fig. 3c).[46] In addition to the relative lattice matching between vertically aligned $BA_2MA_{n-1}Sn_nI_{3n+1}$ and the (100) facet of $MAPb_{0.5}Sn_{0.5}Br_3$, it was showed that the stronger ionic bond between metal-halide and inorganic slabs in vertically aligned structure, in comparison with the weak Van der Waals force in parallel aligned structures, also enables the thermodynamically stable and favorable orientation. These results demonstrated the tunability of 2D perovskite orientation through lattice matching design and growth kinetic control. Lei et al further reported that the 2D crystals grown on (110) facet of 3D perovskites form a rugged surface due to the orientation change. This type of facet-dependent growth has also been reported in the parallel aligned 2D/3D heterojunctions. The growth of 2D crystals based on (200) or (112) facets of 3D perovskites exhibited a templated growth mechanism that the orientations of 2D perovskite match with the 3D facets (Fig. 3d).[47,48] The feasibility of tunning the orientation of 2D perovskite through 3D perovskite template proved its dissimilarity with pure 2D growth, as the interactions between ligands and 3D perovskite lattice becoming a deterministic factor. Small modifications on the molecular configurations, such as fluorine-substitution, can alter the orientation of 2D crystals to either parallel or random oriented.[49,50] The mechanism behind the orientation change remains unclear, which may be further inspected to build a clear correlation between molecular configuration and crystal orientation.

Another type of orientation refers to the relative in-plane orientation between 2D and 3D stacks. This type of orientation is only discussed when the 2D and 3D structures are parallel aligned in the out-of-plane direction. The ligands on 2D perovskite surface interacts with the surface of 3D perovskite, which was coated with ligands that match with those on 2D perovskite, constructing an ordered interface due to the lattice matching and the molecular interactions of the matched ligands.[51] In other cases when the ligands on interfaces are not matching, the interface structure will be disordered with randomly twisted angles. The ordered interface is essential for surface passivation and favored optoelectronic properties, however, it was not confirmed in most of the device-related reports. Given the polycrystalline nature and complicated surface environment of 3D perovskite thin films, the interface orientation requires further characterization to deepen the understanding of the microstructures. Although the device-related 2D/3D heterojunctions contain the matched ligands in most of the studies, the fast crystallization and formation process in device fabrication could result in kinetic product, which may be disordered. In addition, with the development of 2D/3D heterojunctions, new types of heterostructures are emerging, like the low dimensional 2D perovskite with different metal cations[22], which present the possibility of incorporating unmatched ligands on 2D and 3D surfaces in the future.

2.4 Morphological characteristics of 2D/3D heterojunctions

Another scenario at the 2D/3D heterojunction is the interface contact. Achieving conformal coating of 2D perovskite atop of 3D perovskite usually requires the 2D layer to be thin enough, otherwise the stable 2D crystals will grow into large unoriented flakes, which results in poor contact with the 3D perovskite surface.[52] This issue can be addressed by modulating the ligand configurations and adjust the 2D perovskite lattice strains.[53] The increased bulkiness of organic ligands leads to more lattice distortion and octahedra tilting, subsequently increasing the lattice strains, which inhibits the growth of large flakes, instead promoting the conformal coating of 2D crystal on multigrain 3D perovskite surface. Furthermore, the bulkiness and solubility of the organic ligands can also vary the relative location of 2D perovskite with respect to 3D perovskite thin film, such as creating 2D perovskite at the bottom of 3D perovskite thin films spontaneously.[54] Thus, engineering the ligand configuration may be used in controlling the crystallization process, both in a mixed precursor solution or during the surface reconstruction process.

3. Photophysical characteristics of 2D/3D heterojunction

The photophysical properties in 2D/3D heterojunctions are essential for their applications in photovoltaics and other optoelectronic devices. Due to the vitally important role of carrier dynamics in determining the device performance, it has attracted tremendous attention. As discussed in earlier section, the molecular configuration of spacer ligands can be tuned to manipulate the structural characteristics of 2D/3D heterojunctions, it also influences defect passivation, energy level alignment, and then the carrier dynamics in both 2D perovskite and 2D/3D heterojunction. Understanding the influential factors of carrier dynamics at heterointerfaces is equally important as developing strategies to tune structures and gain control over the properties.

3.1. Trap state passivation

Non-radiative recombination, caused by the trap states, is one of the major factors that results in charge transfer loss at heterointerfaces. One of the major goals of designing 2D/3D heterojunction is to reduce the defect-induced interface recombination between 3D perovskite and the charge transporting layer. Among various molecular passivators, the ammonium-functionalized organic cation is a typical type of passivator to coordinate with negatively charged defects.[8,55] Time-resolved microwave conductivity has been used to probe the carrier lifetime and the defect-induced recombination rate at 2D/3D heterojunction formed with BABr ligand.[56] 2D/3D heterostructures exhibit the elongated carrier lifetime, suggesting a reduced recombination loss in comparison with 3D perovskite. However, there is also a report claiming the 2D/3D heterostructure can result in increased electronic disorder in certain situation, causing exponential decrease in charge-carrier mobility.[57] The extrinsic deep trap states generated during the 2D perovskite formation process can exacerbate the non-radiative charge recombination, which becomes a trade-off effect of 2D perovskite.[58] Nevertheless, reducing the surface defects and eliminating non-radiation recombination at surface is the widely accepted role of 2D/3D heterojunction. However, the differences in passivation mechanism between heterojunctions and pure ammonium functionalized organic cations are still unclear. A recent study exhibited a new concept that the band structure of 2D/3D heterojunction is mainly responsible for the ultralow interfacial recombination.[59] The formation of 2D/3D heterojunction results in band bending at the surface of 3D perovskite, which repels the charge carriers from the defective surface, therefore, reducing the interfacial recombination rate. This result indicates that the reduced defect densities on 3D perovskite surface may not be the dominant reasons of reduced recombination rate, while the energy band structures can have more significant impact on carrier dynamics.[27] The optimized energy level offset between 2D and 3D perovskite has also been calculated to increase the tolerance of interfacial defects, further demonstrating the importance of energy levels at the heterojunctions.[60]

3.2. Energy level alignment

Since 2D perovskite is formed with alternated organic and inorganic layers, which defines its low dimensionality, the quantum confinement effect influences its electronic structure and enlarges the bandgap of this type of materials.[30] Thus, 2D/3D heterojunction is usually formed between wide bandgap and narrow bandgap semiconductors. Either a type-II[54,61,62] or type-I[22,29,63,64] energy alignment could be formed at this heterojunction. There is still no consensus on the type of energy alignment formed at 2D/3D heterojunctions. Type-I alignment indicates that the 2D perovskite can reduce the surface non-radiative recombination, while type-II alignment facilitates charge transfer and spatial separation of electrons and holes, which is desired for most of the device structures.

View Article Online
DOI: 10.1039/D4CC02299H

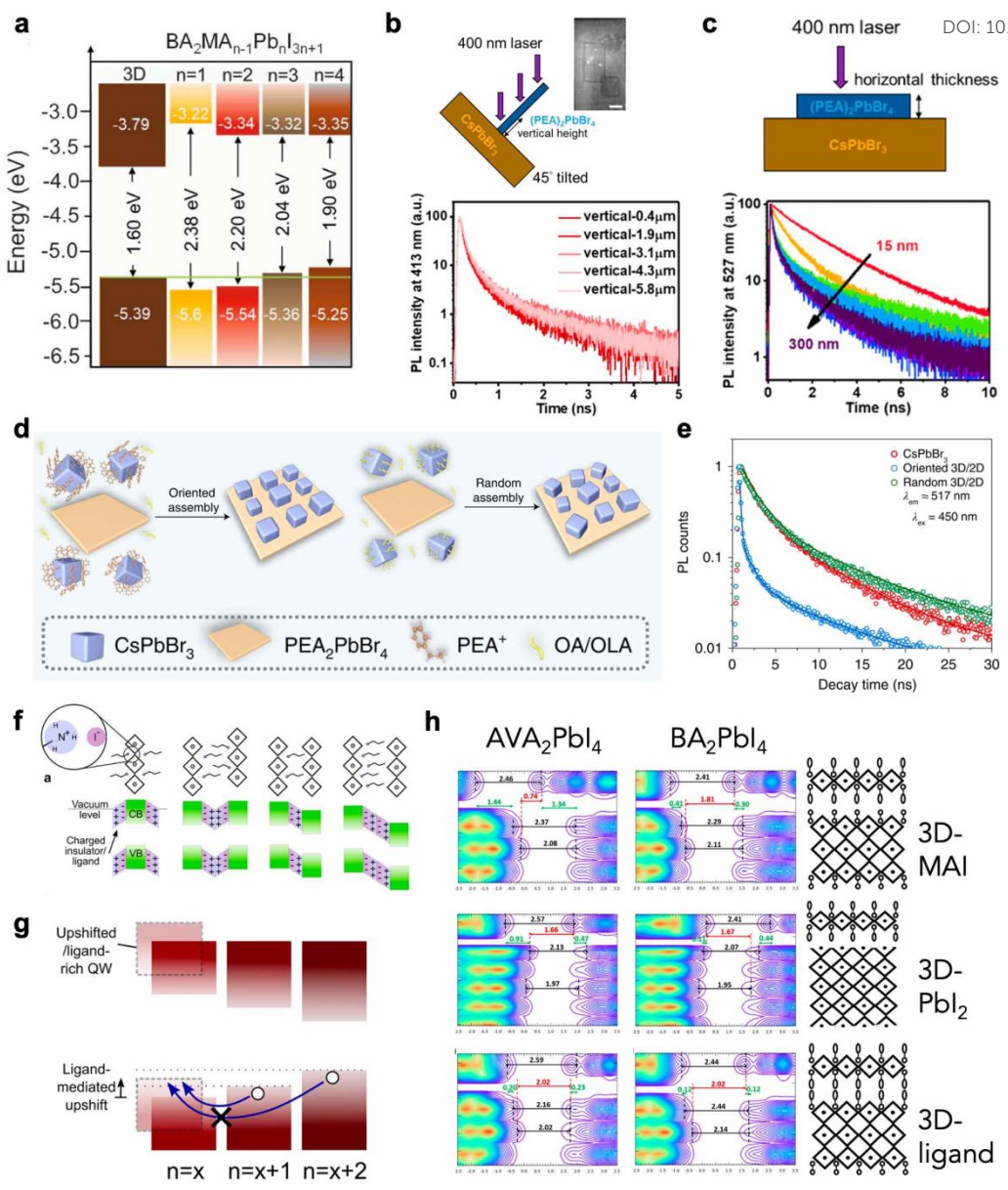

Fig. 4 (a) Energy-level alignment of 3D and BA-based 2D perovskites with different n values.[24] (b) Scheme of vertically aligned $(PEA)_2PbBr_4$ on $CsPbBr_3$ heterostructure (top) and TRPL of the 2D emission in these heterostructure collected at different vertical heights (bottom). (c) Scheme of horizontally aligned 2D/3D heterostructure (top) and TRPL spectra of the emission from $CsPbBr_3$ with varying 2D perovskite thickness (bottom).[66] (d) Scheme of $CsPbBr_3$/$(PEA)_2PbBr_4$ heterostructures via oriented or random assembly. (e) TRPL spectra of the emission from $CsPbBr_3$ in heterostructures.[51] (f) Scheme of the dipole moments in 2D perovskite ligands misalign the energy levels of neighboring 2D phase. (g) Type-II interfaces resulted from the ligand-induced band upshifts.[68] (h) Density of states and the band alignments of 2D/3D heterostructures with different 3D perovskite surface terminations and 2D perovskite ligands.[70]

The *n* value can determine the bandgap of 2D perovskite, but more importantly it influences the relative energy levels between 3D and 2D perovskites. Increasing the *n* value will shrink the bandgap of 2D perovskite, as well as change type-I alignment to type-II alignment in certain scenarios (Fig. 4a).[24] The typical method of constructing 2D/3D heterojunction is by spin coating the ligand solution onto 3D perovskite thin films, and converting the surface of 3D perovskite into 2D structure through cation exchange. The mixed phases resulted from this type of construction method makes it challenging to control the energy landscapes. Efforts have been devoted to achieve type-II alignment at 2D/3D heterojunction through controlling the phases of 2D perovskite based on device engineering and ligand configurations.[23,24] Since conventional and inverted device architectures require hole extraction or electron extraction at the top surface, respectively, different type-II alignments are required. While hole extraction through proper energy alignment of 2D/3D heterojunction has been widely studied and used in devices with conventional architecture, new strategies for constructing 2D perovskites to facilitate electron extraction has just emerged. Usually, increasing the *n* values of 2D perovskite will have more significant effect on the conduction band energy level, which is critical for electron extraction.[23,25]

View Article Online
DOI: 10.1039/D4CC02389H

The charge carrier dynamics also varies according to the 2D perovskite orientations in the heterojunctions, due to the anisotropic properties.[30,65] The 3D $CsPbBr_3$ single crystal thin film and the solution-grown $(PEA)_2PbBr_4$ have been used to demonstrate the orientation effect of 2D perovskite in the heterojunction.[66] Vertically aligned 2D perovskite flake on $CsPbBr_3$ promote efficient charge transfer (Fig. 4b), while horizontally aligned 2D flakes modulate the energy alignment based on the layer thickness (Fig. 4c), as confirmed by the time-resolved photoluminescence (TRPL). Thin 2D flake exhibits type-I alignment, but thicker 2D flake (>150 nm) is more likely to behave as type-II alignment, and facilitates more efficient charge transfer. Since the orientation of 2D perovskites changes the defect density and charge transport efficiency, the omission in considering these features could cause discrepancies in the actual roles of heterojunctions.

As the orientation of the heterojunction also includes in-plane orientation and lattice matching between 3D and 2D perovskites, Zhu and co-workers unveiled the mechanism of carrier dynamics influenced by these factors.[51] They have developed an epitaxial welding method to control the in-plane orientation (Fig. 4d), and demonstrated that the ordered interfaces with matched lattice parameters reduce the lattice strain and improve the charge carrier transfer at the interfaces (Fig. 4e). Owing to the limitation of current 2D/3D model, this type of disordered heterojunction has not been considered in device applications, but needs to be investigated urgently to approach to the theoretical limit of device performance.[67]

As enormous empirical efforts have been invested in controlling energy alignment at heterojunction, there lacks a principle that can guide the design of heterojunction to achieve a proper energy alignment, as the scenarios differ case-by-case. It is due to the variety of heterojunction composition, the lack of advanced techniques to probe the accurate energy levels at the interfaces precisely, but also be caused by the complicated chemical environment on the surface. For example, without a perfect interface between 2D and 3D perovskites, ligand density in between can vary. As the surface charge density is known to shift the effective work function of the material, the various amount of ligand cations subsequently change the energy alignments at 2D/3D heterojunction (Fig. 4f-g).[68] Although, the calculation showed that the ligand-ligand interaction is thermodynamically favored in comparing with the interactions between ligand and other 3D fragment terminated with MA or PbI_2,[52] it is challenging to avoid forming other types of interfaces during the rapid growth process of 2D/3D heterojunction. Recently, Traoré has developed a computational methodology to inspect the energy alignment at 2D/3D heterojunction with $CsPbI_3$ and $(PEA)_2PbI_4$, in consideration of all different factors, including the termination and relaxation of 3D perovskite surface, the passivation effect and dipole formation.[69] It was demonstrated that the interplay between dipoles of different systems can lead to the readjustment of energy level alignment at interfaces, with respect to the energy levels obtains from each individual system. The calculation methods have also been developed to examine the energy level alignment between $(BA)_2PbI_4$ or $(AVA)_2PbI_4$ (AVA = protonated aminovaleric acid) 2D perovskite and $MAPbI_3$, and clearly showed that the surface termination of $MAPbI_3$ and the confined dipole of ligands play critical roles in determining the energy alignment.[70] $(BA)_2PbI_4$ always forms type-II alignment with $MAPbI_3$ but with alternated band-edge position regards the termination of 3D perovskite, while $(AVA)_2PbI_4$-$MAPbI_3$ interfaces could change from type-I to type-II alignment with respect to different terminations (Fig. 4h). Although there still lacks experimental verification, the surface-environment-induced dipole change in 3D perovskite thin films already rise challenges in designing predictable energy alignment at the heterojunction.

Beside these static chemical structure, the light illumination can also alter the charge behavior at the heterojunction. It was reported that the 2D perovskite exhibited light-induced lattice contraction, due to the flexibility of the organic cations and the hole accumulation under illumination, which surmounted the charge transfer problems in 2D perovskites.[71] Special heterostructure has also been designed to insert 2D layer at the grain boundaries of 3D perovskite thin film, and the photogenerated charge carriers have been observed to fill the interfacial traps under illumination, and subsequently increase the built-in potential at interfaces and block electron transfer.[72] On the other hand, the built-in potential facilitates hole extraction from 3D perovskite to 2D perovskite, which indicates the structure can be effectively applied between perovskite and hole transporting layer in solar cell devices to support hole extraction. Owing to this uncommon photoinduced phenomena, the charge carrier dynamics characterized with different techniques under various conditions, such as light-activated spectra, should be considered carefully. There is also report demonstrating the strong Coulomb coupling between the different perovskite n phases due to their overlap of the wave functions, promoting ultrafast carrier transfer rate of <100 fs.[73] The unexpected ultrafast interfacial charge transfer and the compatibility of energy and charge transfer at these heterojunctions explained the reason that they can be used to realize high-performance solar cell devices and LED devices at the same time.

3.3. Carrier dynamics in pure 2D perovskite

Another parameter that influences the charge transfer properties at heterojunction is the carrier dynamics of 2D perovskite itself, as efficient charge transfer in 2D perovskite avoids charge accumulation and recombination at interfaces. The out-of-plane charge transfer in 2D perovskite can be considered as a tunnelling process between inorganic layers, mediated by the organic interlayer. The tunnelling distance and height are coequally important in determining the charge transfer properties. The distance can simply be tuned by the length of spacer ligands, or changes between DJ phase and RP phase. For instance, DJ phases are expected to show excellent carrier transmission properties, due to its shortened interlayer distances, eclipsed stacking arrangement, and enhanced coupling between Pb-I inorganic layers.[74–76] Therefore, the DJ phase 2D perovskites in 2D/3D heterojunctions also exhibited improved charge transfer ability.[61] In contrast, the barrier height is more complicated. In general, two main characters could attune the barrier height: the electronic coupling between the neighboring ligands, and the energy level alignment between the inorganic perovskite layer and the organic spacer layer. Functional groups on the spacer ligands, such as fluorination of PEA,[77,78] and other halide modified ligands,[37] alternate the formation energy, and change the stacking geometry of the organic spacers from face-to-edge to face-to-face through hydrogen bonding (Fig. 5a), subsequently enhancing the interlayer

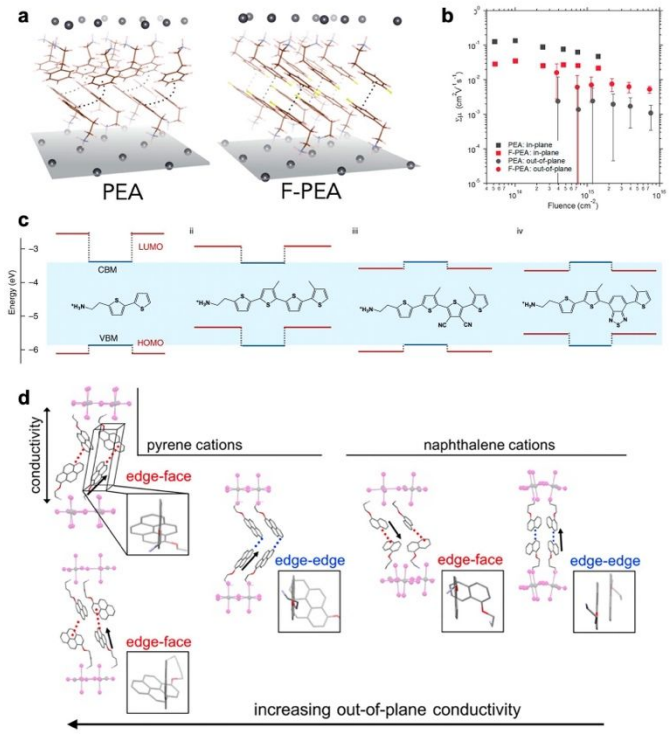

Fig. 5 (a) The structures of $(PEA)_2PbI_4$ and $(F\text{-}PEA)_2PbI_4$ 2D perovskite single crystals. (b) Time resolved microwave conductivity of out-of-plane and in-plane carrier transport in 2D perovskite thin films with different ligands.[77] (c) The energy level alignments of organic (red lines) and inorganic (blue lines) layers within the 2D perovskites with different conjugated ligands.[80] (d) The influence of ligand stacking in 2D perovskites on the out-of-plane conductivity.[85]

electronic coupling (Fig. 5b). The energy level alignment is usually tuned through introducing conjugated molecules into the spacer ligands, to achieve the matched energy levels between organic and inorganic layers.[79] As initially designed and studied by Mitzi, and recently extensively explored by Dou, the organic semiconductor induced 2D perovskites can be constructed to form either type-I or type-II energy alignment between inorganic and organic layers with modified conjugated thiophene or selenophene ligands.[37,80–83] The carrier dynamics depends vitally on the energy level alignment, exhibiting light emission from either Pb-I layer or organic layer, or quenching of the emission due to charge separation (Fig. 5c). It has also been proved that the organic-semiconductor-incorporated 2D perovskite can lead to long-lived charge-separated state over nanosecond time scale due to the type-II alignment.[84] In addition, the conjugated ligands also modify the hydrogen bondings and the supramolecular π-stackings between them, results in excellent out-of-plane conductivity from both aspects (Fig. 5d).[37,85] Further modification in the conductivity and optoelectronic properties can be achieved through designing charge transfer complexes in the organic layer, such as combining the charge-donating and charge-accepting molecules.[86,87]

The in-plane charge transfer mainly occurs within the inorganic perovskite layer, for which the organic spacers do not participate directly. However, the intermolecular interactions between the organic molecules, both in-plane and out-of-plane, influences the octahedra tilting in the inorganic lattice, therefore affecting the in-plane charge transfer properties. As reported by Yao et al, the significant increase in the in-plane carrier mobility of Sn-based 2D perovskite can be achieved through manipulating the molecular configuration of the conjugated ligands.[81] The bandgaps and hole mobilities can also be tuned by equipping the spacer ligands with chemical moieties that can interact with the ammonium group on the adjacent ligand across the organic bilayer.[39]

4. Solar cell devices with 2D/3D heterojunctions

The construction of 2D/3D heterostructures has contributed to an increased number of high-efficiency devices, due to grain boundary passivation, energy landscape management, and stability enhancement. There are two ways to introduce 2D/3D heterostructures in PSCs. One method involves mixing the precursor of 2D perovskite and 3D perovskite together to form a phase segregated 2D/3D heterostructures in bulk perovskite spontaneously.[88] The other method is to deposit 2D perovskite capping layer on top of 3D perovskite thin film to adopt a planar 2D/3D heterostructure as a post-treatment. The later one is usually adopted to avoid the formation of quasi-2D perovskite and limit the amount of 2D perovskite in the bulk material. But the specific treating process still depends on the ligands and formation energy of 2D perovskites. The ligand's molecular configuration is of great importance in tuning the structure properties and optoelectronic properties of the heterostructures, and plays a key role in determining the device performance. The following section is a diagram of several strategies for enhancing the device performance through the molecular-tuned structure and photophysical characteristics of 2D/3D heterojunctions.

4.1. DJ phase 2D perovskite in heterostructure

While RP phase is the most commonly used structure for 2D/3D solar cell devices, the ACI phase has also been used occasionally.[89] Comparing with them, DJ-phase 2D perovskite materials, owing to its smaller interlayer distances and expected excellent charge transfer properties, represent another important type of 2D perovskite in 2D/3D heterostructure that can be applied to PSCs. Commonly used diammonium cations include aliphatic ethane-1,3-diammmonium (EDA), butane-1,3-diammmonium (BDA), octane-1,3-diammmonium (ODA), and aromatic 3-(aminomethyl)piperidinium (3-AMP), etc.[90–96] One of the best performing DJ-phase 2D/3D PSCs features a metastable alternating head to tail capping layer, achieving the highest efficiency up to 24.7% (Fig. 6a).[61] The use of asymmetric organic cation N,N-dimethyl-1,3-propane diammonium (DMePDA), which contains a primary ammonium terminus and a tertiary ammonium terminus with less-stable packing geometry in 2D structure, demonstrated a weakened hydrogen bonding interaction. This effect leads to uplifted valence band maximum for organic layer, and decreases the band offset between the inorganic framework and the organic moieties, improving the hole transport from both shortened charge tunnelling distance and decreased energy barriers.

Among the aromatic diammonium cations, which have more rigid structures and potential π-interactions between organic layers, pyridine functionalized ligands and (phenylene)di(ethylammonium) (PDEA) are the most widely studied in 2D/3D heterojunctions. Adopting the pyridine units, 3-aminomethylpyridine (3-AMPY) and 4-aminomethylpyridine (4-AMPY) was reported to form DJ-phase on

View Article Online
DOI: 10.1039/D4CC02299H

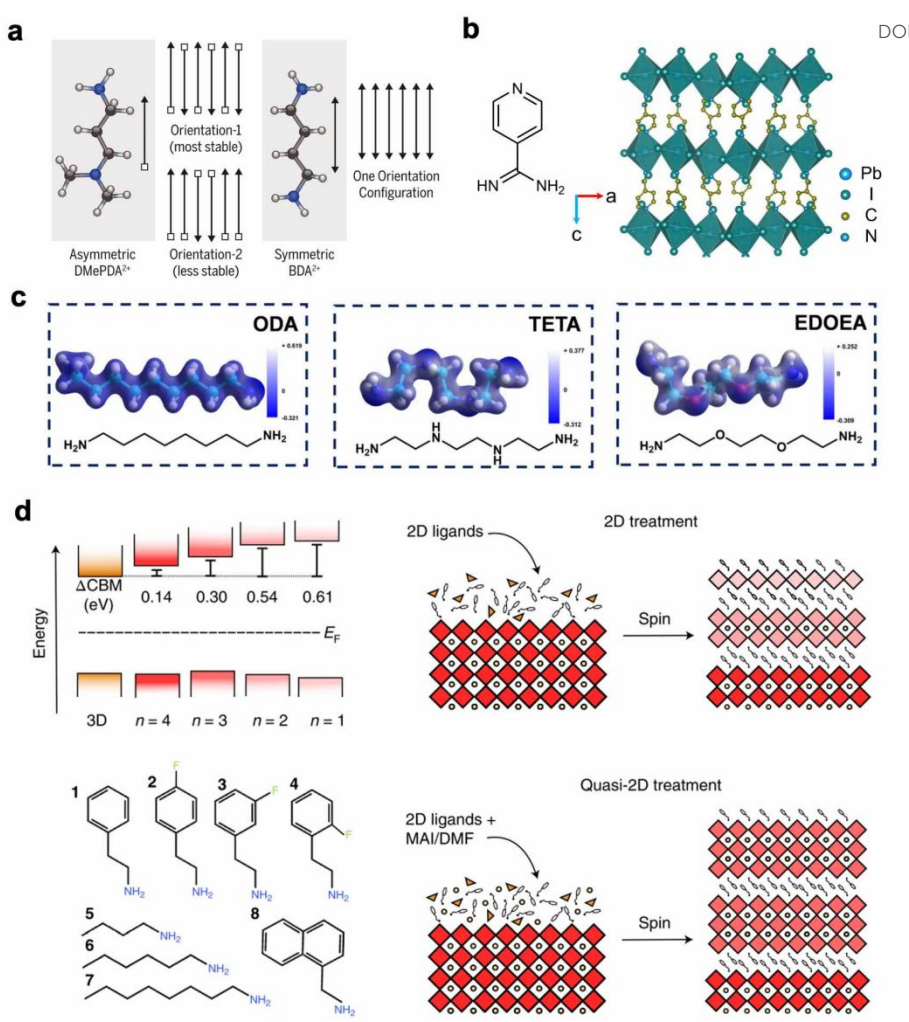

Fig. 6 (a) Two possible arrangements of asymmetric $DMePDA^{2+}$ cations and the only arrangement of symmetric BA^{2+} cations.[61] (b) The molecular structure of 4AP and single crystal structure of $(4AP)PbI_4$.[97] (c) The molecular structures of ODA, TETA and EDOEA, and their corresponding electron-density distributions.[99] (d) Band alignment of 3D and 2D perovskites with different *n* values and the ligands used in the study (left), and the scheme of 2D and quasi-2D treatment process (right).[23]

top of 3D perovskite, with smaller conduction band offset between 2D and 3D perovskites compared with its RP phase analog.[21] Assisted with the solvent engineering, the reconstruction of perovskite surface with 3-AMPY results in uniform and large *n* value in DJ phases, favorable band alignment and elongated electron diffusion length which facilitate the efficient electron tunnelling. With further development of $FAPbI_3$-based PSCs, the lattice matching between amino group on the organic ligand and the $FAPbI_3$ lattice becomes critical. 4-amidinopyridine (4AP) with the unique amidino terminus, which matches with the crystal lattice based on FA^+ cations, was first reported in DJ-based 2D perovskite for the formation of 2D/3D heterostructures in PSCs (Fig. 6b).[97] According to the in-situ photoluminescence (PL) spectra study, $(4AP)PbI_4$ assists the nucleation and helps decrease the voids and defect densities of 3D perovskite. The highest PCE can reach to 24.9% for conventional devices. Similarly, an in-situ surface reaction was found by using 3-AMPY, which generates pyridine-based ligands with similar formamidinium terminus after reacting with surface FA cation.[98] However, the n-type doping from the surface engineering plays a key role in the devices rather than forming 2D/3D heterostructures

Introducing heteroatom in the aliphatic chain of diammonium cations can change the intermolecular interactions, and subsequently tune the inorganic lattice tilting angles, and help to build high-performance PSCs. EDOEA (Fig. 6c) with oxygen heteroatom was used to form phase pure *n*=1 DJ-phase microcrystals vertically aligned at the grain boundaries of 3D perovskites.[40] The minimization of photo-generated charge carrier localization in 2D perovskite by phase pure structure demonstrated a champion efficiency of 21.06% in $MAPbI_3$-based solar cells. Later on, a more comprehensive study was performed, and explained the regulation of charge transfer properties through the octahedra tilting of inorganic octahedra when different heteroatoms, i.e. N in TETA and O in EDOEA, interacts with $[PbI_6]^{2-}$ framework.[99] A deeper understanding of binding energy and hydrogen bonds in different ligands revealed that EDOEA is the most suitable one for high-quality perovskite, yielding triple-cation based device efficiency up to 22.68%.

4.2 2D perovskite *n* phase modulation in heterojunction

The *n* values of 2D perovskite is another significant characteristic that influence the performance of PSCs. It has been found that the n

View Article Online
DOI: 10.1039/D4CC02290H

values can be tuned by molecular engineering approach due to formation energy differences.[23,50] Especially, the wider layer width is preferred when translating the 2D/3D heterostructure from conventional devices to inverted devices, because of the electron-blocking nature of low width *n*=1 perovskite. BA was found to be able to form phase pure *n*=2 perovskite capping layers when directly spin coated on 3D perovskite surface, but the 3-fluoro-phenethylammonium (3F-PEA) can preferentially form mainly *n*=3 2D layers with the MAI addition, superior to BA- or PEA-based 2D or quasi-2D perovskites (Fig. 6d). The reduce energy barrier for electron extraction allowed a PCE of 23.91% for inverted PSCs. The formation energy calculation for high-*n* value PEA- and F-PEA-based 2D perovskites in this study made a compensation of earlier calculation on the *n*=1 2D perovskite,[78] providing a full spectrum of the possibility of forming different types of 2D perovskites.

4.3 2D orientation modulation in heterojunction

The orientation control in 2D PSCs is one of the most critical factors that influences the device efficiency, as vertical alignment of 2D perovskite increases the charge transfer efficiency by magnitudes. However, the situation in 2D/3D heterojunction differs from pure 2D devices. While the fluorination of PEA has been found to be able to tune the 2D perovskite orientation on top of 3D perovskite, the device results demonstrated that the parallel oriented 2D perovskite, formed with PEA, exhibited better defect passivation effect, while the randomly oriented F-PEA-2D perovskite showed limited effect of passivation.[49,50] However, a recent study claimed that the obliquely oriented DJ-phase 2D perovskite, templated grown from (110) facet of $MAPbI_2Br$, exhibited enhanced solar cell performance in comparing with the parallel oriented 2D crystal due to the improved charge transfer property.[48] It remains controversial whether the vertically aligned or parallel aligned 2D crystal is favourable for the device performance of 2D/3D solar cells, and a careful study is needed, taking all factors, including the *n*-phase purity, orientation and energy alignment, into consideration.

4.4 Energy level alignment with conjugated ligands

Ligands with single aromatic ring, like PEA,[26] F-PEA,[23,77] pentafluoro-phenylethylamine (FEA)[100] and thiophene-ethylamine (TEA) cations[101], are firstly reported to passivate the surface defect and control the crystallization process. The small molecular nature allows them to form 2D/3D heterostructures easily, but the strategy of manipulating energy level alignment at the interface is limited. Using conjugated cations as ligands allows tuning the energy level alignment in 2D perovskite quantum wells, as well as in 2D/3D heterojunctions. However, increasing the conjugation also sizing up the organic components, making it crucial to balance between conjugation and the ability to form 2D perovskite. From the molecular design perspective, increasing the number of phenyl or thiophene units can narrow the band gap and shift the valence band maximum (VBM) of 2D perovskites.[79,102] Ma et. al. designed a multifunctional capping layer (MCL) with quater-thiophene backbone (4Tm) in conventional solar cells (Fig. 7a and 7b).[103] This 2D/3D interface modifier upshifted VBM and efficiently improved hole extraction from perovskite layers, which also retarded the interfacial non-radiative decay via charge recombination. As a result, the device efficiency has improved from 19.94% to 22.06%. Similarly, by increasing the phenyl conjugation, a two-ring naphthalene-based

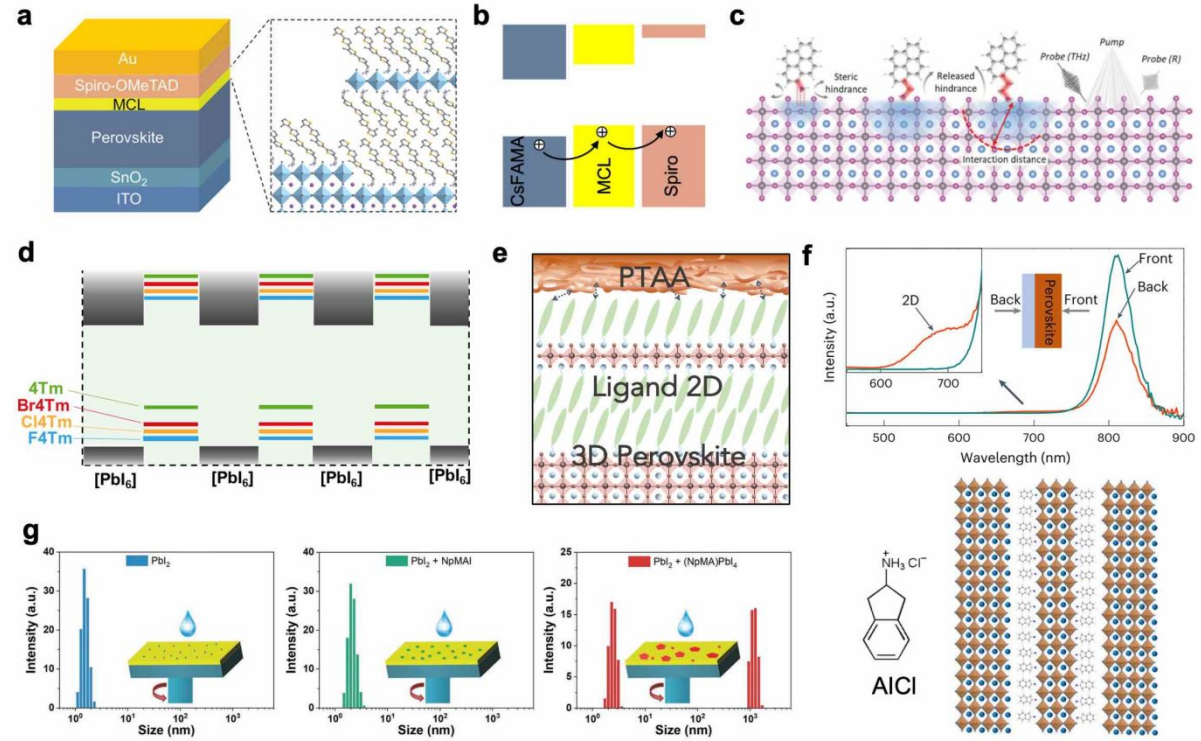

Fig. 7 (a) The structure of perovskite solar cell device based on the MCL-modified interface and schematic illustration of the MCL structure. (b) Energy level alignment and charge transfer direction.[103] (c) Scheme of the influence of ligand alkyl chain length on the interaction distance.[105] (d) Energy level alignments between inorganic and organic layers within the 2D perovskite formed with conjugated ligands.[37] (e) Scheme of 2D perovskite structure between PTAA and 3D perovskite.[53] (f) PL spectra of the 2D/3D perovskite thin films obtained from different incident directions (top), and the scheme of 2D structures formed with AICl (bottom).[54] (g) Aggregation size distribution in precursor solutions of PbI_2 mixed with either NpMA or $(NpMA)_2PbI_4$.[111]

View Article Online DOI: 10.1039/D4CC02991J

ligand, 1-naphthylmethylammonium bromide (NMABr), was used to construct type-II alignment at the 2D/3D interface and the highest efficiency reached to 21.09%.[104] Further enlarging the phenyl conjugation, recently Xue et. al. reported pyrene-based A-site cations for tuning the electronic state at band edge (Fig. 7c),[105] although the crystal structure of pyrene-based 2D perovskites was not new and can date back as early as 1900s.[106] Through the tuning of alkyl chain length, the molecular intercalation distance of pyrene can be adjusted to optimize electronic coupling, in which ethyl chain demonstrated the best performance with a PCE of 23.0%.

Beside increasing the number of conjugated rings, electron-withdrawing halogen substitution has been proven to be another efficient approach to achieve delicate band offset adjustment of 2D/3D heterostructure (Fig. 7d).[37] Fluoro-, chloro-, and bromo-4Tm were designed and synthesized based on 4Tm through halogenation reactions using N-fluorobenzenesulfonimide, N-chlorosuccinimide and N-bromosuccinimide reagents, respectively. For Cl4Tm, the smallest energy level offset was observed at the 2D/3D heterojunctions, and the as-formed solar cells demonstrated the optimized performance with PCEs up to 24.6%. Another critical factor contributing to performance enhancement is the improved out-of-plane conductivity, resulting from interlayer halogen interaction, evident by the conductive atomic force microscope (cAFM) and microwave-conductivity characterization.

While the 2D/3D heterostructure is widely adopted in fabricating PSCs for the electronic state management, the surface homogeneity of 2D capping layer is often overlooked, despite its crucial role in inhibiting ion migration and enhancing the environmental stability. By adjusting the side-chain of the quater-thiophene backbone, it was observed that changes occurred not only in the physical solubility of ligand molecules, but also in the growth dynamics and morphology of 2D/3D heterostructures.[53] For 4Te ligand, which replaces the methyl groups on 4Tm with ethyl groups, the solubilizing ethyl side-chain and the bulkiness increase the lattice strain in 2D perovskite, and then lead to the formation of more uniform 2D perovskite coating rather than segregated islands of 2D crystals. Further, due to the conformal 2D layers in the 2D/3D heterostructure, the binding between polymer hole-transporting layer poly (triaryl amine) (PTAA) and bulk 3D perovskite is strengthened, evident from mechanical peeling test (Fig. 7e). As of now, the exploration of large, conjugated cations used in 2D/3D heterostructures is still limited, and there is a lack of guidelines for new ligand design. More exotic structures and detailed analyses that lead to new material development are still needed in this field.

4.5 Perovskite thin film structure modulation

Molecular configuration and its corresponding 2D/3D heterostructure can further influence the devices with respect to the properties of the bulk perovskite materials and the bottom interfaces. For bulk perovskite optimization, anions in ammonium salts can not only serve as additives for surface work function adjustment, such as octylammonium tosylate on 3D perovskite, but also tune the crystallization and dimensionality of low-dimensional perovskite, as seen in neo-pentylammonium (neoPA) chloride, bromide and iodide.[107,108] In addition, acids such as β-guanidinopropionic acid (β-GUA) and 4-guanidinobutanoic acid (GBA) can also function as crystallization control additives when incorporated into bulk perovskites, and form 2D/3D heterostructures at the same time.[109,110] Buried interfaces can be improved by forming 2D crystal seeds at the bottom, which regulated the growth of 3D perovskite. Li et al. reported the employment of 2-aminoindan hydrochloride (AICl) at the buried interface (Fig. 7f).[54] Because of the poor solubility of AICl, the pre-existing nucleates in 3D perovskite precursors manipulated the crystallization process and improved the film quality. Similarly, in sequential deposition method of 3D perovskite, 1-naphthalenemethylammonium (NpMA) with the form of 2D structure can be introduced to the PbI_2 precursor layer, and followed by cation deposition, which enlarged grain size of 3D perovskite crystals (Fig. 7g).[111] Overall, it is encouraged to pursue a series of molecular designs, and to draw more comprehensive conclusion and in-depth understanding through systematic studies. This approach should not be limited to a specific device configuration or one "super" molecule.

5. Light-emitting diode device with 2D/3D heterojunctions

The 2D and quasi-2D perovskites have been widely used in light-emitting device fabrication, due to their quantum confinement properties, high photoluminescence quantum yields, and tunable emission spectra. However, with further development, the need for light emission from 3D perovskite layer initiated the need of designing efficient and stable 3D perovskite LEDs. Therefore, the perovskite 2D/3D heterojunction structure rises up.

The role of 2D/3D heterojunctions in current LED devices mainly focuses on defect passivation of 3D perovskite surfaces.[112–115] Phenylalkylammonium iodide were firstly reported to be applied on 3D perovskite LEDs to reduce surface defect density and suppress iodide ion migration through the steric and Coulomb interactions of the passivating molecules.[115] Although, no 2D structures were observed, the report did not deny the possibility of forming ultrathin 2D perovskites. Other reports clearly showed the formation of 2D perovskites on top of 3D crystals with phenyl-based ammonium salt.[112,113] It was reported that through a proton transfer method to introduce benzylamine onto the 3D perovskite surface (Fig. 8a), the 2D perovskite crystallized without destroying the bottom 3D structures, and effectively suppressed the formation of trap states and ion migration, enhancing the efficiency (Fig. 8b and 8c).[112] Beside tuning the 3D perovskite emission wavelength through composition change,[116] the quantum confinement strategy can also be applied to the 3D perovskite thin film through introducing PEA-based 2D perovskites, which passivated the 3D perovskite surface, and simultaneously shrink the grain size and lowered the emission wavelength.[113,117] A record champion external quantum efficiency (EQE) of 12.3% at 478 nm with 3D perovskite was achieved.

In addition to the trap state passivation, the energy level alignment of 2D/3D perovskite structure is also a critical factor for efficient radiative recombination of electrons and holes within the emission materials. Different from the solar cell devices, a gradient n phase in LED device can generate energy cascade channels to induce the

View Article Online
DOI: 10.1039/D4CC02299H

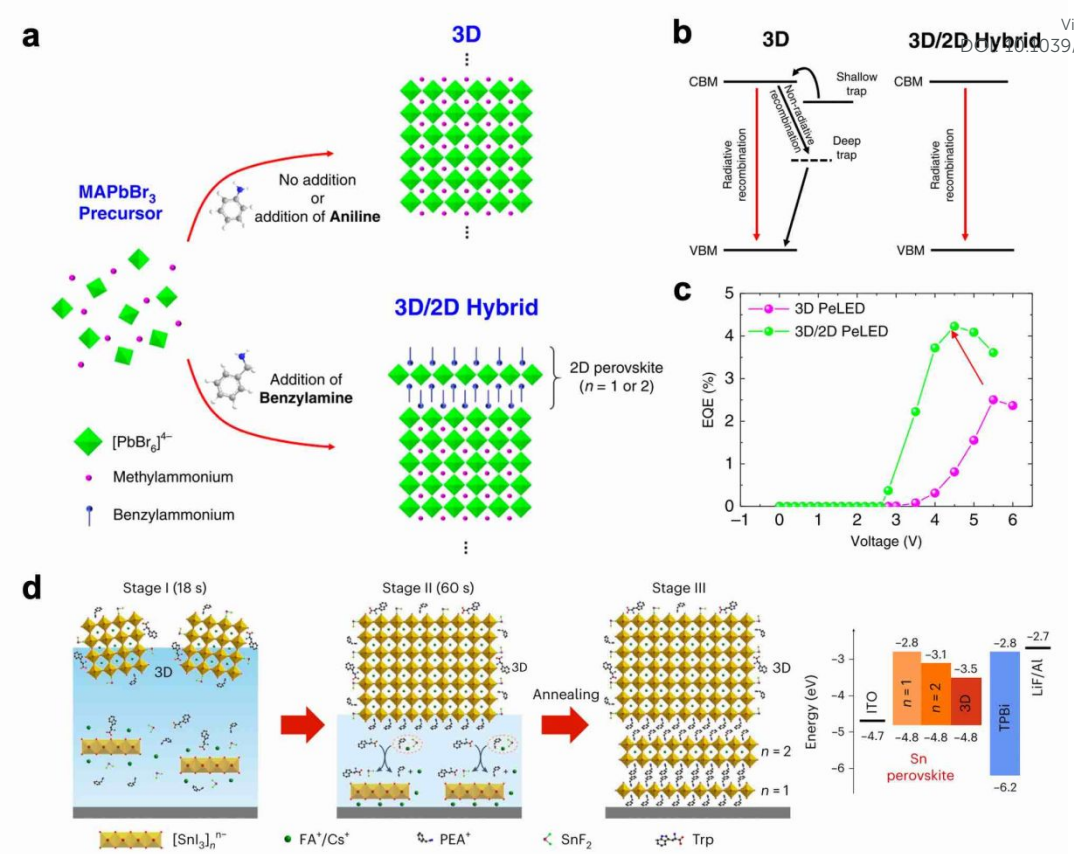

Fig. 8 (a) Scheme of surface treatment of 3D perovskites with benzylamine through proton transfer, or with aniline. (b) Scheme of the charge carrier dynamics in pure 3D and 2D/3D hybrid structures. (c) External quantum efficiency (EQE) of the pure 3D and 2D/3D hybrid LED devices.[112] (d) Scheme of the crystallization pathway of epitaxially grown 2D/3D heterojunction (left), and the energy level alignment (right).[114]

charge transfer from 2D to 3D phase, and increase the densities of injected electrons and holes. It was reported that the mixture of PEABr and guanidinium bromide (GABr) as organic ligands can generate cascade channels while also improve defect passivation effect.[118] With proper energy alignment between 2D and 3D perovskites, the hole transporting layer in the device can even be replaced by 2D perovskite layer.[114] Min et al have developed the method to directly spin coat epitaxially grown 2D/3D heterojunction in Sn-based LED devices, created an interface with matched out-of-plane and in-plane lattice alignment, minimizing the interface defect density and performing efficient hole transfer (Fig. 8d). As a result, this hole-transporting-layer-free device exhibited a EQE of 11.6% for near-infrared emission.

Currently, the study of 2D/3D heterojunction in LED devices is underdeveloped, while most of the studies are still focusing on conventional ligands such as PEA[113,114,116,117] and BA,[119,120] with occasional exploration on other benzamidine and NMA ligand.[121,122] We are expecting more of the ligand types that are used in the construction of 2D perovskite LEDs will be adopted in the 2D/3D heterojunction systems.

6. Photodetector with 2D/3D heterojunctions

The application of perovskite in photodetector requires low defect density to reduce dark current and increase the sensitivity to light. Therefore, single crystal perovskite is frequently used, due to its low defect density in the bulk material.[123,124] The construction of 2D/3D heterostructure is another strategy of lowering the defect density on the surface of the crystal. He et al reported a facile and universal strategy of growing $(FPEA)_2PbBr_4$ structure epitaxially on the surface of $FAPbBr_3$ single crystal, to passivate the defects and prevent ion migration, resulting in a lower detectable X-ray dose.[125] Others also reported the formation of 2D/3D heterojunctions, either through epitaxial welding or in-situ growing, can lead to improved stability while achieving ultra-low detection limit for X-ray detectors.[126,127] The proper energy level alignment further lower the barrier for electron transfer. Similar as the solar cell devices, the 2D phase has also been used to tune the bottom interface of 3D perovskite to reduce the defect density and improve the energy alignment in the photodiode.[128,129] Later on, a more comprehensive study has demonstrated the advantages of creating a 2D-3D gradient structure, and modulated the energy alignment of this multidimensional perovskite film through ligand selection.[130] Ligands including BA, PEA and cyclohexylmethylammonium (CMA) were investigated to illustrate their preferential in forming 2D structures with different *n*-phases, at bottom or on top of 3D crystals, vertical or parallel orientations, and the energy alignments were subsequently tuned with respect to the energy level of electron blocking layer. The optimized heterostructure exhibited the record low dark current and

View Article Online
DOI: 10.1039/D4CC02280H

increased photosensitivity. In addition to the typical PEA or BA ligands, the TEA ligands has also been adopted in the formation of 2D/3D heterostructure, to take the advantage of interactions between S and Pb atoms to modulate the crystallization process.[131]

Another important topic in photodetector is the polarization-sensitive photodetection. The anisotropic nature of 2D perovskite and its tunability with various organic ligand selection make it promising candidate for polarized light detection. However, limited by the absorption anisotropy and inhibited carrier transport in 2D perovskites, the polarization sensitivity is still low. Construction of 2D/3D heterojunction with chiral-2D perovskites allows enhanced optical absorption, increased free carrier densities, and effective charge separation due to the built-in electric field at the heterojunction.[132] Therefore, AMP-based 2D perovskites, with a chiral component, has been used to construct single crystal 2D/3D heterojunction, and exhibited extremely high polarization sensitivity up to 17.6.[133]

7. 2D/3D heterojunction degradation mechanism and stability challenges

One of the major goal of applying 2D/3D heterostructures in optoelectronic devices is to improve the device stability. Up to now, many reports demonstrated improved device stabilities with this type of heterostructures, such as maintained 95% of its initial efficiency for over 1000 hr damp-heat test,[25] or achieved T_{99} of >2000 hr.[24] The inorganic perovskite solar cells even sustained the accelerated aging test under the temperature as high as 110°C, with the assistance of inorganic $Cs_2PbI_2Cl_2$ 2D layer surface passivation.[134] These achievements are mainly due to the reduced defect densities, aligned energy levels which avoid charge accumulation at interfaces, or the suppressed ion migration across the interfaces.[25] Although the moisture stability of the devices can be effectively achieved through modulating the hydrophobicity and chain length of the ligand,[100,135,136] it can also be realized through outstanding encapsulation and is not an issue as severe as the intrinsic stability. However, there are quite diverse results in the reports about the intrinsic stability of the 2D/3D heterostructures under different aging conditions. The bulky organic ligands are prone to intercalate into the perovskite lattice, and it is the method that most reports adopted to form the 2D structures atop of 3D thin films. However, it also indicates that the organic cation can migrate and break the stable structures of 3D perovskites. The advanced techniques, such as low electron–fluence, four-dimensional scanning transmission electron microscopy and nanobeam electron diffraction have been applied to identify the organic cation migration and lattice reconstruction at 2D/3D heterojunction, providing crucial evidences of the dynamic nature of 2D/3D interfaces.[137] During the aging process, whether the reconstruction of interface will benefit or be detrimental to the device performance is still unknown, and has not been reported in the earlier studies.[138,139]

Perini et al performed a thorough investigation on the thermal stability of the 2D/3D PSCs with some of the most commonly used spacer ligands, PEAI and octylammonium bromide (OABr).[140] The 2D/3D solar cell devices all exhibited a sudden drop in performance at the initial aging stage, followed with an extended lifetime afterwards. This type of effect was attributed to the reconstruction of interface layer during the thermal aging process, which did not occur in the control devices. After the construction stage in which the bulky ligands formed 2D perovskites, continuous thermal aging will further change the 2D structure, reducing the crystallinity and induce new types of trap states, till the structure reaches to a thermodynamically stable state (Fig. 9a). Different ligands can go through different reconstruction process, due to the steric effect, interactions between ligands and perovskite compositions, and the stability of 2D phases.[141,142] Alkyl ammoniums like OA or BA tend to accumulate on the top surface, while aryl ammoniums such as PEA or FPEA have relatively uniform depth distribution, and may penetrate deeper into perovskite lattice.[143] Therefore, OA-based structure exhibits improved thermal stability in comparing with PEA-based 2D/3D heterostructure, which is known as a detrimental passivator for thermal stability test (Fig. 9b).[26]

Due to the intercalation and reconstruction issue of 2D/3D heterojunction under thermal stress, especially with 85°C thermal stability test, other ammonium passivators have been developed to avoid the formation of 2D perovskite phases, such as the fluorinated aniliniums (Fig. 9c).[143,144] It has been reported that tuning the substitution site of $PDEAI_2$ gives different formation energy of DJ-phase 2D perovskites.[144] The most steric hinderance one, ortho-PDEAI2, has the smallest tendency of forming DJ-phase 2D perovskite, and prevent the ligand from entering the perovskite lattice, showing excellent passivation effects and enhanced stability, better than the para-$PDEAI_2$ which is prone to form traditional DJ-phase 2D phase. Other methods have also been adopted to inhibit the ion diffusion across the interfaces through inserting cross-linked polymers between 2D and 3D phases.[145] However, these strategies diminished the important advantage of tuning energy level alignment through 2D/3D heterojunction. New types of 2D phase ligands are required to inhibit reconstruction of the perovskite surface during thermal aging process. For example, the photochemically cross-linked 2D/3D heterojunction, formed with 4-vinylbenzylammonium (VBA) ligand, could be a promising candidate to suppress ion migration during aging process (Fig. 9d).[146] The ligands were connected into an in-plane polymer chain structure after the 2D perovskite is formed, which could impede the diffusion of small ligands. The steric organic ammonium salt, nortropinone iodide, has also been introduced to the interface and increased the steric hinderance to migration, but through forming a 1D/3D heterojunction instead of 2D/3D structure.[147] A secondary amine has also been used to form 2D/3D heterostructure and exhibited improved thermal stability due to the strong intermolecular interactions, although more crystallographic studies have to be performed to confirm the structures.[148] The conjugated ligands have been demonstrated to significantly suppress anion migration in 2D perovskite, in both out-of-plane and in-plane direction.[149–151] With their bulky size and steric hinderance effect, they are expected to impede the 2D/3D heterojunction reconstruction, but still can be designed to form stable 2D perovskite with excellent electronic properties, which are excellent candidate for ligands to solve the stability issues.

View Article Online
DOI: 10.1039/D4CC02299H

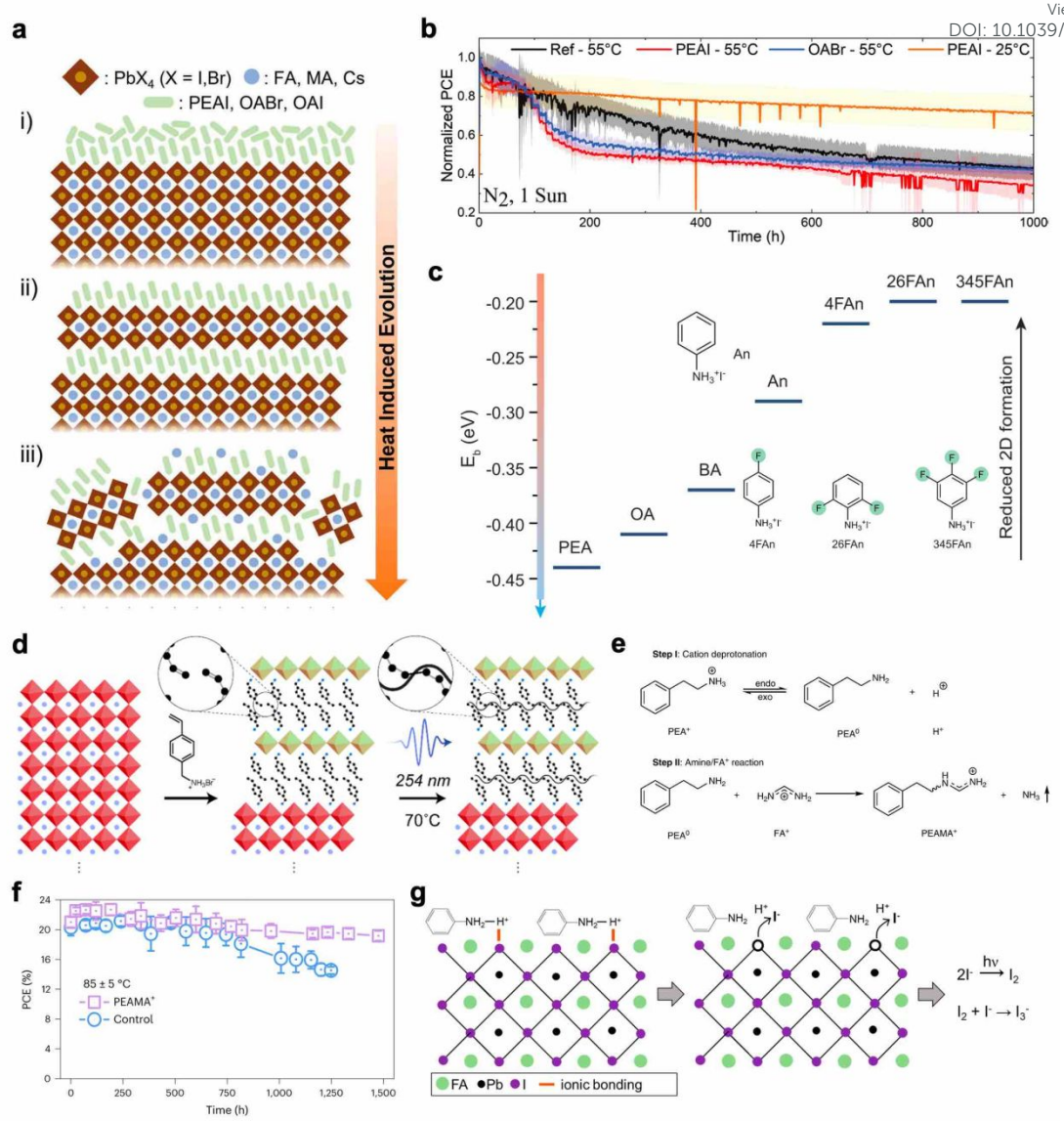

Fig. 9 (a) Scheme of the evolution of the 2D/3D heterostructure treated with bulky cations upon annealing. (b) The maximum power point tracking of different 2D/3D devices measured under various temperatures.[140] (c) The binding energy calculated for ammonium ligands substituted into $MAPbI_3$ perovskite slabs, and the structure of anilinium.[143] (d) Scheme of the formation process of cross-linked 2D perovskite atop of 3D phase using VBA cations.[146] (e) Chemical reactions between PEA^+ and FA^+. (f) The device stability of control and $PEAMA^+$ devices measured under 85°C and 1 sun illumination.[152] (g) Chemical reaction between perovskite surface and anilinium.[153]

Another new degradation mechanism induced by 2D/3D heterostructure is the degradation of organic ligand itself. With the development of $FAPbI_3$-based PSCs, the reaction between FA^+ cations and ligands become an issue. The reaction between FA^+ cation and 3-AMPY to form MPyFA$^+$ (N-(3-methylpyridine) formamidinium), was firstly used as a passivation strategy to smooth the surface energy levels of 3D perovskite thin films.[98] However, the reaction was found later on to also occur between FA^+ cation and commonly used 2D phase ligands such as PEA^+ and BA^+ at 85 °C under illumination.[152] The ligands with low acid dissociation constant (pK_a) can easily be deprotonated and react with FA^+ cation, forming methaniminium and releasing ammonia (Fig. 9e), which damages the perovskite surfaces and grain boundaries, severely limits the high-temperature photostability of these 2D/3D PSCs. New ammonium cations with high pK_a was developed through directly adopting the (phenethylamino)methaniminium ($PEAMA^+$, pK_a =12.0) as passivation ligand and enhanced the device thermal stability (Fig. 9f). The pK_a values of a diverse of other ammonium cations have been investigated, clearly showing that cyclohexylammonium chloride (CYCl) with a pK_a of 10.6 exhibited lowest free iodide generation under illumination, best device efficiency, and longer lifetime (Fig. 9g).[153] Nevertheless, all these ammonium cations with high pK_a values have not been demonstrated as forming stable 2D perovskite structures.

8. Summary and outlook

Leveraging the high efficiency and good stability already achieved with 2D/3D heterostructure in PSCs, it is still going to be one of the most promising strategies for the commercialization of PSCs, and will also be the important next step for the development of perovskite LEDs and photodetectors. We have discussed about how the ligand

configuration influences the structural characteristics in 2D/3D heterojunction, including phase space, thickness of inorganic perovskite layer, the orientation of 2D perovskite and the morphology of 2D/3D heterojunction. We have also systematically reviewed the photophysics at 2D/3D heterojunctions, including the influencing factors and modulation of the carrier dynamics through ligand configurations, which pave the way for efficient device applications. The understanding of structural and photophysical characteristics directly impacts the device performance when these heterostructures are adopted into solar cells, light emitting devices or photodetectors. A vast amount of reports have shown the advantages of 2D/3D heterojunctions in devices, which improves efficiencies and stabilities through passivating trap states, managing energy level alignments and suppressing ion migrations. While the representative strategies have been reviewed, we also raised the awareness of current problems encountered in the device application about the unclear degradation mechanism and arguable stability. Here we briefly proposed a few research directions that needs further investigation and development to set solid foundation for the future stable and efficient PSCs:

(1) As theoretical calculation have demonstrated critical role of atomic-scale interfacial chemical environment for the energy alignment of 2D/3D heterojunction, there's a desire to develop advanced characterization techniques to probe it experimentally. The influencing factors include but not limited to the termination plane of 3D perovskite, the amount of ligands inserted at interfaces, the ligand cation dipole. The omissions in considering all these factors could be one of the causes for the discrepancies of the type of energy alignment existing in 2D/3D heterojunctions. Building a framework that can predict the interfacial energy alignment with the consideration of all these factors, will not only unify the current energy alignment model, but also lead to the surface pretreatment to modulate the surface chemical environment and support the future design of new ligands.

(2) The 2D/3D heterojunctions are mainly built on the top of 3D perovskite thin films, owing to the relative ease of surface treatment process. However, the microstructures and energy alignment at the bottom interfaces proved their importance in the efficiency and stability of PSCs.[154–156] The creation of 2D/3D heterojunction at the bottom interfaces began to unlock its potential in the field.[29,54] However, it remains challenging to develop a non-disruptive method to grow the 3D perovskite atop of the 2D crystals with high qualities. Thermal evaporation for 3D thin film growth is one strategy, but diminishes the advantage of low-cost with solution process. Given enormous opportunities the organic molecules offered and their roles in manipulating the crystallization process of 3D perovskites, new design rules will emerge to generate new types of ligands which either spontaneously form 2D structures at the bottom during the global crystallization process of 3D perovskite, or avoid the dissolution by solvent during the 3D phase growth.

(3) With the emphasis on the stability of PSCs, previously hidden problems of 2D/3D heterojunction are brought to the surfaces, and new ligand designs will be needed to solve those problems. As mentioned before, the dynamic nature of 2D/3D heterostructure causes reconstruction and degradation during thermal and illumination aging process. The new type of ligands that have high pK_a to lower down the reactivity, and low penetration depth to avoid migration, will guide the field to achieve significantly improved device stability, while still maintain the energy alignment benefit of 2D/3D heterojunctions.

(4) Fully exploring the potential of conjugated ligands may be leveraged to tune the structural and optoelectronic properties of 2D perovskites. The conjugated ligand is a special group of ligands that participate the energy alignment of 2D perovskites directly, instead of regulating the inorganic layers, which gives it wider window in changing the optoelectronic properties. While the current strategy controls the *n*-phases of 2D structures for lowering down the electron transporting barriers at interfaces between perovskite and electron transporting layer in the inverted device structures, the conjugated ligands may have the capability of diminishing the energy barrier and changing to reverse type-II alignment to facilitate electron transport at this interfaces. The bulkiness and the rigidness of conjugated ligands will also easily regulate the lattice distortion and formation energy of 2D perovskites, subsequently control the growth kinetics and morphology of 2D/3D heterostructures. The current challenge for widespread applications of this strategy is the synthetic difficulties that requires an easy pathway. The machine-learning algorithm will emerge and reduce the working load of organic synthesis, guiding the further exploration.

(5) Expanding the library of 2D perovskite materials and structures will be another avenue towards engineering the 2D/3D interface energy levels and other carrier dynamics properties. The surface treatment strategy of 2D/3D heterostructure developed from cation exchange with ligand solutions to the full precursor solution or vapor phase deposition methods, which enabled more possibility for composition and structure modulation of the capping 2D perovskites. For example, incorporating metal cations other than Pb^{2+}/Sn^{2+} allowed stronger n–N isotype heterojunctions and improved built-in potential.[22] Introducing the all-inorganic 2D perovskite structure into the all-inorganic perovskite solar cells created a new type of 2D/3D heterojunction, and provided extraordinary stability performance.[134] With the discovery of other stable facets,[157] the corresponding 2D perovskites suiting for different facets may also need to be developed to catch up with the conventional (100) facet, and new group of bulky organic ligands will be desired.

In summary, a comprehensive understanding of the atomic-level structure of 2D/3D heterojunction will mature the strategy, and continued research and advancement in the new ligand configurations to fulfill for more desires will guide the field to achieve high-performance device in both efficiency and stability.

Author Contributions

Writing and editing of the manuscript: K.M. and J.S. Supervision: L.D. and K.M.

Conflicts of interest

There are no conflicts to declare.

Data availability

No primary research results, software or code have been included and no new data were generated or analysed as part of this review.

Acknowledgements

The authors acknowledge funding support from the Solar Energy Technologies Office under the U.S. Department of Energy with the Award DE-EE0009519.

Notes and references

1 A. Kojima, K. Teshima, Y. Shirai and T. Miyasaka, *J. Am. Chem. Soc.*, 2009, **131**, 6050–6051.
2 L. Zhen, L. Bo, W. Xin, S. S. A., Z. Shoufeng, G. Danpeng, L. N. J. and Z. Zonglong, *Science*, 2022, **376**, 416–420.
3 J. Suo, B. Yang, E. Mosconi, D. Bogachuk, T. A. S. Doherty, K. Frohna, D. J. Kubicki, F. Fu, Y. Kim, O. Er-Raji, T. Zhang, L. Baldinelli, L. Wagner, A. N. Tiwari, F. Gao, A. Hinsch, S. D. Stranks, F. De Angelis and A. Hagfeldt, *Nat. Energy*, 2024, **9**, 172–183.
4 R. Lin, Y. Wang, Q. Lu, B. Tang, J. Li, H. Gao, Y. Gao, H. Li, C. Ding, J. Wen, P. Wu, C. Liu, S. Zhao, K. Xiao, Z. Liu, C. Ma, Y. Deng, L. Li, F. Fan and H. Tan, *Nature*, 2023, **620**, 994–1000.
5 J. Park, J. Kim, H.-S. Yun, M. J. Paik, E. Noh, H. J. Mun, M. G. Kim, T. J. Shin and S. Il Seok, *Nature*, 2023, **616**, 724–730.
6 O. Almora, D. Baran, G. C. Bazan, C. I. Cabrera, S. Erten-Ela, K. Forberich, F. Guo, J. Hauch, A. W. Y. Ho-Baillie, T. J. Jacobsson, R. A. J. Janssen, T. Kirchartz, N. Kopidakis, M. A. Loi, R. R. Lunt, X. Mathew, M. D. Mcgehee, J. Min, D. B. Mitzi, M. K. Nazeeruddin, J. Nelson, A. F. Nogueira, U. W. Paetzold, B. P. Rand, U. Rau, H. J. Snaith, E. Unger, L. Vaillant-Roca, C. Yang, H. Yip and C. J. Brabec, *Adv. Energy Mater.*, 2023, **13**, 2203313.
7 L. Jin-Wook, T. Shaun, S. S. Il, Y. Yang and P. Nam-Gyu, *Science*, 2022, **375**, eabj1186.
8 D. Luo, R. Su, W. Zhang, Q. Gong and R. Zhu, *Nat. Rev. Mater.*, 2020, **5**, 44–60.
9 Z. Ni, C. Bao, Y. Liu, Q. Jiang, W.-Q. Wu, S. Chen, X. Dai, B. Chen, B. Hartweg, Z. Yu, Z. Holman and J. Huang, *Science*, 2020, **367**, 1352–1358.
10 Y. Xia, C. Zhao, P. Zhao, L. Mao, Y. Ding, D. Hong, Y. Tian, W. Yan and Z. Jin, *J. Power Sources*, 2021, **494**, 229781.
11 L. Qin, M. Zhu, Y. Xia, X. Ma, D. Hong, Y. Tian, Z. Tie and Z. Jin, *Nano Res.*, 2024, **17**, 5131–5137.
12 G. Grancini and M. K. Nazeeruddin, *Nat. Rev. Mater.*, 2019, **4**, 4–22.
13 L. Mao, C. C. Stoumpos and M. G. Kanatzidis, *J. Am. Chem. Soc.*, 2019, **141**, 1171–1190.
14 F. Zhang, H. Lu, J. Tong, J. J. Berry, M. C. Beard and K. Zhu, *Energy Environ. Sci.*, 2020, **13**, 1154–1186.
15 X. Zhao, T. Liu and Y. Loo, *Adv. Mater.*, 2022, **34**, 2105849.
16 T.-H. Han, K. Y. Jang, Y. Dong, R. H. Friend, E. H. Sargent and T.-W. Lee, *Nat. Rev. Mater.*, 2022, **7**, 757–777.
17 J. Yan, W. Qiu, G. Wu, P. Heremans and H. Chen, *J. Mater. Chem. A*, 2018, **6**, 11063–11077.
18 P. Gao, A. R. Bin Mohd Yusoff and M. K. Nazeeruddin, *Nat. Commun.*, 2018, **9**, 5028.
19 W. Huang, Y. Wang and S. K. Balakrishnan, *Chem. Commun.*, 2018, **54**, 7944–7947.
20 B. Singh, N. G. Saykar, B. S. Kumar, D. Afria, S. C. K. and S. R. Rondiya, *ACS Omega*, 2024, **9**, 10000–10016.
21 S. Ramakrishnan, D. Song, Y. Xu, X. Zhang, G. Aksoy, M. Cotlet, M. Li, Y. Zhang and Q. Yu, *Adv. Energy Mater.*, 2023, **13**, 2302240.
22 S. Ye, H. Rao, M. Feng, L. Xi, Z. Yen, D. H. L. Seng, Q. Xu, C. Boothroyd, B. Chen, Y. Guo, B. Wang, T. Salim, Q. Zhang, H. He, Y. Wang, X. Xiao, Y. M. Lam and T. C. Sum, *Nat. Energy*, 2023, **8**, 284–293.
23 H. Chen, S. Teale, B. Chen, Y. Hou, L. Grater, T. Zhu, K. Bertens, S. M. Park, H. R. Atapattu, Y. Gao, M. Wei, A. K. Johnston, Q. Zhou, K. Xu, D. Yu, C. Han, T. Cui, E. H. Jung, C. Zhou, W. Zhou, A. H. Proppe, S. Hoogland, F. Laquai, T. Filleter, K. R. Graham, Z. Ning and E. H. Sargent, *Nat. Photonics*, 2022, **16**, 352–358.
24 S. Sidhik, Y. Wang, M. De Siena, R. Asadpour, A. J. Torma, T. Terlier, K. Ho, W. Li, A. B. Puthirath, X. Shuai, A. Agrawal, B. Traore, M. Jones, R. Giridharagopal, P. M. Ajayan, J. Strzalka, D. S. Ginger, C. Katan, M. A. Alam, J. Even, M. G. Kanatzidis and A. D. Mohite, *Science*, 2022, **377**, 1425–1430.
25 A. Randi, U. Esma, S. Akmaral, A. Faisal, S. A. S., L. Jiang, H. G. T., N. M. I., E. M. K., B. Maxime, C. Yuan, X. Fuzong, A. T. G., R. A. Ur, W. Chien-Lung, A. T. D., S. Udo, D. B. Michele, A. Erkan and D. W. Stefaan, *Science*, 2022, **0**, eabm5784.
26 Q. Jiang, Y. Zhao, X. Zhang, X. Yang, Y. Chen, Z. Chu, Q. Ye, X. Li, Z. Yin and J. You, *Nat. Photonics*, 2019, **13**, 460–466.
27 Y.-W. Jang, S. Lee, K. M. Yeom, K. Jeong, K. Choi, M. Choi and J. H. Noh, *Nat. Energy*, 2021, **6**, 63–71.
28 J. Wen, Y. Zhao, P. Wu, Y. Liu, X. Zheng, R. Lin, S. Wan, K. Li, H. Luo, Y. Tian, L. Li and H. Tan, *Nat. Commun.*, 2023, **14**, 7118.
29 R. Azmi, D. S. Utomo, B. Vishal, S. Zhumagali, P. Dally, A. M. Risqi, A. Prasetio, E. Ugur, F. Cao, I. F. Imran, A. A. Said, A. R. Pininti, A. S. Subbiah, E. Aydin, C. Xiao, S. Il Seok and S. De Wolf, *Nature*, 2024, **628**, 93–98.
30 J.-C. Blancon, J. Even, C. C. Stoumpos, M. G. Kanatzidis and A. D. Mohite, *Nat. Nanotechnol.*, 2020, **15**, 969–985.
31 E. S. Vasileiadou, B. Wang, I. Spanopoulos, I. Hadar, A. Navrotsky and M. G. Kanatzidis, *J. Am. Chem. Soc.*, 2021, **143**, 2523–2536.
32 I. Zimmermann, S. Aghazada and M. K. Nazeeruddin, *Angew. Chemie Int. Ed.*, 2019, **58**, 1072–1076.
33 H. Gao, W. Wei, L. Li, Y. Tan and Y. Tang, *J. Phys. Chem. C*, 2020, **124**, 19204–19211.
34 A. Dučinskas, G. Y. Kim, D. Moia, A. Senocrate, Y.-R. Wang, M. A. Hope, A. Mishra, D. J. Kubicki, M. Siczek, W. Bury, T. Schneeberger, L. Emsley, J. V Milić, J. Maier and M. Grätzel, *ACS Energy Lett.*, 2021, **6**, 337–344.
35 D. Pan, Y. Fu, N. Spitha, Y. Zhao, C. R. Roy, D. J. Morrow, D. D. Kohler, J. C. Wright and S. Jin, *Nat. Nanotechnol.*, 2021, **16**, 159–165.

36 J. Y. Park, R. Song, J. Liang, L. Jin, K. Wang, S. Li, E. Shi, Y. Gao, M. Zeller, S. J. Teat, P. Guo, L. Huang, Y. S. Zhao, V. Blum and L. Dou, *Nat. Chem.*, 2023, **15**, 1745–1753.

37 K. Ma, J. Sun, H. R. Atapattu, B. W. Larson, H. Yang, D. Sun, K. Chen, K. Wang, Y. Lee, Y. Tang, A. Bhoopalam, L. Huang, K. R. Graham, J. Mei and L. Dou, *Sci. Adv.*, 2023, **9**, eadg0032.

38 Q. Wei, F. Zhang, X. Li, F. Wu, Z. Yue, J. Luo and X. Liu, *Small*, 2024, **n/a**, 2311969.

39 X. Zhao, M. L. Ball, A. Kakekhani, T. Liu, A. M. Rappe and Y.-L. Loo, *Nat. Commun.*, 2022, **13**, 3970.

40 P. Li, Y. Zhang, C. Liang, G. Xing, X. Liu, F. Li, X. Liu, X. Hu, G. Shao and Y. Song, *Adv. Mater.*, 2018, **30**, 1805323.

41 C. Gong, X. Chen, J. Zeng, H. Wang, H. Li, Q. Qian, C. Zhang, Q. Zhuang, X. Yu, S. Gong, H. Yang, B. Xu, J. Chen and Z. Zang, *Adv. Mater.*, 2024, **36**, 2307422.

42 M. Xiong, W. Zou, K. Fan, C. Qin, S. Li, L. Fei, J. Jiang, H. Huang, L. Shen, F. Gao, A. K.-Y. Jen and K. Yao, *ACS Energy Lett.*, 2022, **7**, 550–559.

43 K. Wang, Z.-Y. Lin, Z. Zhang, L. Jin, K. Ma, A. H. Coffey, H. R. Atapattu, Y. Gao, J. Y. Park, Z. Wei, B. P. Finkenauer, C. Zhu, X. Meng, S. N. Chowdhury, Z. Chen, T. Terlier, T.-H. Do, Y. Yao, K. R. Graham, A. Boltasseva, T.-F. Guo, L. Huang, H. Gao, B. M. Savoie and L. Dou, *Nat. Commun.*, 2023, **14**, 397.

44 S. J. Yang, K. Wang, Y. Luo, J. Y. Park, H. Yang, A. H. Coffey, K. Ma, J. Sun, S. Wieghold, C. Zhu and L. Dou, *ACS Energy Lett.*, 2023, **8**, 3693–3701.

45 J. Seo, K. Wang, A. H. Coffey, G. He, H. Yang, Y. H. Lee, K. Ma, J. Sun, J. Y. Park, H. Zhao, C. Yuan, C. Zhu, M. Y. Sfeir and L. Dou, *Adv. Opt. Mater.*, 2023, **11**, 2301164.

46 Y. Lei, Y. Li, C. Lu, Q. Yan, Y. Wu, F. Babbe, H. Gong, S. Zhang, J. Zhou, R. Wang, R. Zhang, Y. Chen, H. Tsai, Y. Gu, H. Hu, Y.-H. Lo, W. Nie, T. Lee, J. Luo, K. Yang, K.-I. Jang and S. Xu, *Nature*, 2022, **608**, 317–323.

47 G. Uzurano, N. Kuwahara, T. Saito, A. Fujii and M. Ozaki, *ACS Mater. Lett.*, 2022, **4**, 378–384.

48 G. Uzurano, N. Kuwahara, T. Saito, K. Abe, S. Miyake, D. Hishida, Y. Takeoka, A. Fujii and M. Ozaki, *Appl. Phys. Express*, 2023, **16**, 41005.

49 M. E. F. Bouduban, V. I. E. Queloz, V. M. Caselli, K. T. Cho, A. R. Kirmani, S. Paek, C. Roldan-Carmona, L. J. Richter, J. E. Moser, T. J. Savenije, M. K. Nazeeruddin and G. Grancini, *J. Phys. Chem. Lett.*, 2019, **10**, 5713–5720.

50 T. Niu, J. Lu, X. Jia, Z. Xu, M.-C. Tang, D. Barrit, N. Yuan, J. Ding, X. Zhang, Y. Fan, T. Luo, Y. Zhang, D.-M. Smilgies, Z. Liu, A. Amassian, S. Jin, K. Zhao and S. Liu, *Nano Lett.*, 2019, **19**, 7181–7190.

51 Z. Zhu, C. Zhu, L. Yang, Q. Chen, L. Zhang, J. Dai, J. Cao, S. Zeng, Z. Wang, Z. Wang, W. Zhang, J. Bao, L. Yang, Y. Yang, B. Chen, C. Yin, H. Chen, Y. Cao, H. Gu, J. Yan, N. Wang, G. Xing, H. Li, X. Wang, S. Li, Z. Liu, H. Zhang, L. Wang, X. Huang and W. Huang, *Nat. Mater.*, 2022, **21**, 1042–1049.

52 A. H. Proppe, A. Johnston, S. Teale, A. Mahata, R. Quintero-Bermudez, E. H. Jung, L. Grater, T. Cui, T. Filleter, C.-Y. Kim, S. O. Kelley, F. De Angelis and E. H. Sargent, *Nat. Commun.*, 2021, **12**, 3472.

53 J. Sun, K. Ma, Z.-Y. Lin, Y. Tang, D. Varadharajan, A. X. Chen, H. R. Atapattu, Y. H. Lee, K. Chen, B. W. Boudouris, K. R. Graham, D. J. Lipomi, J. Mei, B. M. Savoie and L. Dou, *Adv. Mater.*, 2023, **35**, 2300647.

54 H. Li, C. Zhang, C. Gong, D. Zhang, H. Zhang, Q. Zhuang, X. Yu, S. Gong, X. Chen, J. Yang, X. Li, R. Li, J. Li, J. Zhou, H. Yang, Q. Lin, J. Chu, M. Grätzel, J. Chen and Z. Zang, *Nat. Energy*, 2023, **8**, 946–955.

55 H. Zhang, L. Pfeifer, S. M. Zakeeruddin, J. Chu and M. Grätzel, *Nat. Rev. Chem.*, 2023, **7**, 632–652.

56 F. Yao and Q. Lin, *ACS Photonics*, 2022, **9**, 3165–3171.

57 Z. Yang, J. Lai, R. Zhu, J. Tan, Y. Luo and S. Ye, *J. Phys. Chem. C*, 2022, **126**, 12689–12695.

58 M. Zhang, Y. Sun, X. Wang, J. Gao, H.-Y. Wang, J. Lin, Y. Wang, L.-M. Fu, X.-C. Ai and J.-P. Zhang, *J. Phys. Chem. Lett.*, 2023, **14**, 1934–1940.

59 D. W. deQuilettes, J. J. Yoo, R. Brenes, F. U. Kosasih, M. Laitz, B. D. Dou, D. J. Graham, K. Ho, Y. Shi, S. S. Shin, C. Ducati, M. G. Bawendi and V. Bulović, *Nat. Energy*, 2024, **9**, 457–466.

60 W. Yang, B. Ding, Z. Lin, J. Sun, Y. Meng, Y. Ding, J. Sheng, Z. Yang, J. Ye, P. J. Dyson and M. K. Nazeeruddin, *Adv. Mater.*, 2023, **35**, 2302071.

61 Z. Fei, P. S. Yeon, Y. Canglang, L. Haipeng, D. S. P., X. Chuanxiao, U. Soňa, Z. Xiaoming, D. H. Linze, C. Xihan, W. Xiaoming, M. L. E., S. K. H., S. L. T., T. Glenn, P. Sean, R. E. L., L. Yueh-Lin, B. J. J., B. M. C., Y. Yanfa, L. B. W. and Z. Kai, *Science*, 2021, **0**, eabj2637.

62 T. Zhang, M. Long, M. Qin, X. Lu, S. Chen, F. Xie, L. Gong, J. Chen, M. Chu, Q. Miao, Z. Chen, W. Xu, P. Liu, W. Xie and J. Xu, *Joule*, 2018, **2**, 2706–2721.

63 T. Yang, F. Li, C.-H. Lin, X. Guan, Y. Yao, X. Yang, T. Wu and R. Zheng, *Cell Reports Phys. Sci.*, 2023, **4**, 101447.

64 C. Li, R. Zhu, Z. Yang, J. Lai, J. Tan, Y. Luo and S. Ye, *Angew. Chem.*, 2023, **135**, e202214208.

65 J. Li, J. Ma, X. Cheng, Z. Liu, Y. Chen and D. Li, *ACS Nano*, 2020, **14**, 2156–2161.

66 M.-Y. Kuo, N. Spitha, M. P. Hautzinger, P.-L. Hsieh, J. Li, D. Pan, Y. Zhao, L.-J. Chen, M. H. Huang, S. Jin, Y.-J. Hsu and J. C. Wright, *J. Am. Chem. Soc.*, 2021, **143**, 4969–4978.

67 H. Duim, H.-H. Fang, S. Adjokatse, G. H. ten Brink, M. A. L. Marques, B. J. Kooi, G. R. Blake, S. Botti and M. A. Loi, *Appl. Phys. Rev.*, 2019, **6**, 31401.

68 R. Quintero-Bermudez, A. H. Proppe, A. Mahata, P. Todorović, S. O. Kelley, F. De Angelis and E. H. Sargent, *J. Am. Chem. Soc.*, 2019, **141**, 13459–13467.

69 B. Traoré, P. Basera, A. J. Ramadan, H. J. Snaith, C. Katan and J. Even, *ACS Energy Lett.*, 2022, **7**, 349–357.

70 A. Mahata, E. Mosconi, D. Meggiolaro and F. De Angelis, *Chem. Mater.*, 2020, **32**, 105–113.

71 W. Li, S. Sidhik, B. Traore, R. Asadpour, J. Hou, H. Zhang, A. Fehr, J. Essman, Y. Wang, J. M. Hoffman, I. Spanopoulos, J. J. Crochet, E. Tsai, J. Strzalka, C. Katan, M. A. Alam, M. G. Kanatzidis, J. Even, J.-C. Blancon and A. D. Mohite, *Nat. Nanotechnol.*, 2022, **17**, 45–52.

72 D. Yu, F. Cao, J. Liao, B. Wang, C. Su and G. Xing, *Nat. Commun.*, 2022, **13**, 6229.

73 K. Wei, T. Jiang, Z. Xu, J. Zhou, J. You, Y. Tang, H. Li, R. Chen, X. Zheng, S. Wang, K. Yin, Z. Wang, J. Wang and X. Cheng, *Laser Photon. Rev.*, 2018, **12**, 1800128.

74 P. Li, X. Liu, Y. Zhang, C. Liang, G. Chen, F. Li, M. Su, G. Xing, X. Tao and Y. Song, *Angew. Chem.*, 2020, **132**, 6976–6981.

75 Y. Dong, X. Dong, D. Lu, M. Chen, N. Zheng, R. Wang, Q. Li, Z. Xie and Y. Liu, *Adv. Mater.*, 2022, **35**, 2205258.

76 T. Sheikh, V. Nawale, N. Pathoor, C. Phadnis, A. Chowdhury and A. Nag, *Angew. Chemie Int. Ed.*, 2020, **59**, 11653.

77 F. Zhang, D. H. Kim, H. Lu, J.-S. Park, B. W. Larson, J. Hu, L. Gao, C. Xiao, O. G. Reid, X. Chen, Q. Zhao, P. F. Ndione, J. J. Berry, W. You, A. Walsh, M. C. Beard and K. Zhu, *J. Am. Chem. Soc.*, 2019, **141**, 5972–5979.

78 J. Hu, I. W. H. Oswald, S. J. Stuard, M. M. Nahid, N. Zhou, O. F. Williams, Z. Guo, L. Yan, H. Hu, Z. Chen, X. Xiao, Y. Lin, Z. Yang, J. Huang, A. M. Moran, H. Ade, J. R. Neilson and W. You, *Nat. Commun.*, 2019, **10**, 1276.

79 J. Sun, K. Wang, K. Ma, J. Y. Park, Z.-Y. Lin, B. M. Savoie and L. Dou, *J. Am. Chem. Soc.*, 2023, **145**, 20694–20715.

80 Y. Gao, E. Shi, S. Deng, S. B. Shiring, J. M. Snaider, C. Liang, B. Yuan, R. Song, S. M. Janke, A. Liebman-Peláez, P. Yoo, M. Zeller, B. W. Boudouris, P. Liao, C. Zhu, V. Blum, Y. Yu, B. M. Savoie, L. Huang and L. Dou, *Nat. Chem.*, 2019, **11**, 1151–1157.

81 Y. Gao, Z. Wei, P. Yoo, E. Shi, M. Zeller, C. Zhu, P. Liao and L. Dou, *J. Am. Chem. Soc.*, 2019, **141**, 15577–15585.

82 E. Shi, S. Deng, B. Yuan, Y. Gao, Akriti, L. Yuan, C. S. Davis, D. Zemlyanov, Y. Yu, L. Huang and L. Dou, *ACS Nano*, 2019, **13**, 1635–1644.

83 Z. Wei, K. Wang, W. Zhao, Y. Gao, Q. Hu, K. Chen and L. Dou, *Chem. Commun.*, 2021, **57**, 11469–11472.

84 S. Deng, J. M. Snaider, Y. Gao, E. Shi, L. Jin, R. D. Schaller, L. Dou and L. Huang, *J. Chem. Phys.*, 2020, **152**, 44711.

85 J. V Passarelli, D. J. Fairfield, N. A. Sather, M. P. Hendricks, H. Sai, C. L. Stern and S. I. Stupp, *J. Am. Chem. Soc.*, 2018, **140**, 7313–7323.

86 J. V. Passarelli, C. M. Mauck, S. W. Winslow, C. F. Perkinson, J. C. Bard, H. Sai, K. W. Williams, A. Narayanan, D. J. Fairfield, M. P. Hendricks, W. A. Tisdale and S. I. Stupp, *Nat. Chem.*, 2020, **12**, 672–682.

87 W. T. M. Van Gompel, R. Herckens, K. Van Hecke, B. Ruttens, J. D'Haen, L. Lutsen and D. Vanderzande, *Chem. Commun.*, 2019, **55**, 2481–2484.

88 Y. Xia, M. Zhu, L. Qin, C. Zhao, D. Hong, Y. Tian, W. Yan and Z. Jin, *Energy Mater.*, 2023, **3**, 300004.

89 Q. Zhuang, H. Li, C. Zhang, C. Gong, H. Yang, J. Chen and Z. Zang, *Adv. Mater.*, 2023, **35**, 2303275.

90 Z. Chen, X. Zheng, F. Yao, J. Ma, C. Tao and G. Fang, *J. Mater. Chem. A*, 2018, **6**, 17625–17632.

91 M. D. Malouangou, Y. Yang, Y. Zhang, L. Bai, J. T. Matondo, M. Mbumba, M. W. Akram and M. Guli, *Mater. Res. Bull.*, 2022, **150**, 111793.

92 L. Mao, W. Ke, L. Pedesseau, Y. Wu, C. Katan, J. Even, M. R. Wasielewski, C. C. Stoumpos and M. G. Kanatzidis, *J. Am. Chem. Soc.*, 2018, **140**, 3775–3783.

93 M. Chen, M.-G. Ju, M. Hu, Z. Dai, Y. Hu, Y. Rong, H. Han, X. C. Zeng, Y. Zhou and N. P. Padture, *ACS Energy Lett.*, 2019, **4**, 276–277.

94 S. Wu, J. Zhang, Z. Li, D. Liu, M. Qin, S. H. Cheung, X. Lu, D. Lei, S. K. So, Z. Zhu and A. K.-Y. Jen, *Joule*, 2020, **4**, 1248–1262.

95 X. Jiang, J. Zhang, S. Ahmad, D. Tu, X. Liu, G. Jia, X. Guo and C. Li, *Nano Energy*, 2020, **75**, 104892.

96 J. Lu, L. Jiang, W. Li, F. Li, N. K. Pai, A. D. Scully, C.-M. Tsai, U. Bach, A. N. Simonov, Y.-B. Cheng and L. Spiccia, *Adv. Energy Mater.*, 2017, **7**, 1700444.

97 T. Yang, C. Ma, W. Cai, S. Wang, Y. Wu, J. Feng, N. Wu, H. Li, W. Huang, Z. Ding, L. Gao, S. (Frank) Liu and K. Zhao, *Joule*, 2023, **7**, 574–586.

98 Q. Jiang, J. Tong, Y. Xian, R. A. Kerner, S. P. Dunfield, C. Xiao, R. A. Scheidt, D. Kuciauskas, X. Wang, M. P. Hautzinger, R. Tirawat, M. C. Beard, D. P. Fenning, J. J. Berry, B. W. Larson, Y. Yan and K. Zhu, *Nature*, 2022, **611**, 278–283.

99 Y. Zhong, G. Liu, Y. Su, W. Sheng, L. Gong, J. Zhang, L. Tan and Y. Chen, *Angew. Chemie Int. Ed.*, 2022, **61**, e202114588.

100 Y. Liu, S. Akin, L. Pan, R. Uchida, N. Arora, J. V Milić, A. Hinderhofer, F. Schreiber, A. R. Uhl, S. M. Zakeeruddin, A. Hagfeldt, M. I. Dar and M. Grätzel, *Sci. Adv.*, 2019, **5**, eaaw2543.

101 Y. Yan, S. Yu, A. Honarfar, T. Pullerits, K. Zheng and Z. Liang, *Adv. Sci.*, 2019, **6**, 1900548.

102 Z.-Y. Lin, J. Sun, S. B. Shiring, L. Dou and B. M. Savoie, *Angew. Chemie Int. Ed.*, 2023, **62**, e202305298.

103 K. Ma, H. R. Atapattu, Q. Zhao, Y. Gao, B. P. Finkenauer, K. Wang, K. Chen, S. M. Park, A. H. Coffey, C. Zhu, L. Huang, K. R. Graham, J. Mei and L. Dou, *Adv. Mater.*, 2021, **33**, 2100791.

104 S. Zhao, M. Qin, H. Wang, J. Xie, F. Xie, J. Chen, X. Lu, K. Yan and J. Xu, *Sol. RRL*, 2020, **4**, 2000282.

105 J. Xue, R. Wang, X. Chen, C. Yao, X. Jin, K.-L. Wang, W. Huang, T. Huang, Y. Zhao, Y. Zhai, D. Meng, S. Tan, R. Liu, Z.-K. Wang, C. Zhu, K. Zhu, M. C. Beard, Y. Yan and Y. Yang, *Science*, 2021, **371**, 636–640.

106 M. Braun, W. Tuffentsammer, H. Wachtel and H. C. Wolf, *Chem. Phys. Lett.*, 1999, **307**, 373–378.

107 S. Tan, T. Huang, I. Yavuz, R. Wang, T. W. Yoon, M. Xu, Q. Xing, K. Park, D.-K. Lee, C.-H. Chen, R. Zheng, T. Yoon, Y. Zhao, H.-C. Wang, D. Meng, J. Xue, Y. J. Song, X. Pan, N.-G. Park, J.-W. Lee and Y. Yang, *Nature*, 2022, **605**, 268–273.

108 X. Liu, T. Webb, L. Dai, K. Ji, J. A. Smith, R. C. Kilbride, M. Yavari, J. Bi, A. Ren, Y. Huang, Z. Wang, Y. Shen, G. Shao, S. J. Sweeney, S. Hinder, H. Li, D. G. Lidzey, S. D. Stranks, N. C. Greenham, S. R. P. Silva and W. Zhang, *ENERGY Environ. Mater.*, 2022, **5**, 670–682.

109 Q. Yao, Q. Xue, Z. Li, K. Zhang, T. Zhang, N. Li, S. Yang, C. J. Brabec, H.-L. Yip and Y. Cao, *Adv. Mater.*, 2020, **32**, 2000571.

110 Z. Wang, Y. Lu, Z. Xu, J. Hu, Y. Chen, C. Zhang, Y. Wang, F. Guo and Y. Mai, *Adv. Sci.*, 2021, **8**, 2101856.

111 T. Zhou, Z. Xu, R. Wang, X. Dong, Q. Fu and Y. Liu, *Adv. Mater.*, 2022, **34**, 2200705.

112 H. Kim, J. S. Kim, J.-M. Heo, M. Pei, I.-H. Park, Z. Liu, H. J.

Yun, M.-H. Park, S.-H. Jeong, Y.-H. Kim, J.-W. Park, E. Oveisi, S. Nagane, A. Sadhanala, L. Zhang, J. J. Kweon, S. K. Lee, H. Yang, H. M. Jang, R. H. Friend, K. P. Loh, M. K. Nazeeruddin, N.-G. Park and T.-W. Lee, *Nat. Commun.*, 2020, **11**, 3378.

113 K. Zhang, Z. Su, Y. Shen, L.-X. Cao, X.-Y. Zeng, S.-C. Feng, Y. Yu, X. Gao, J.-X. Tang and Y. Li, *ACS Nano*, 2024, **18**, 4570–4578.

114 H. Min, N. Wang, N. Chen, Y. Tong, Y. Wang, J. Wang, J. Liu, S. Wang, X. Wu, P. Yang, H. Shi, C. Zhuo, Q. Chen, J. Li, D. Zhang, X. Lu, C. Zhu, Q. Peng, L. Zhu, J. Chang, W. Huang and J. Wang, *Nat. Nanotechnol.*, 2024, **19**, 632–637.

115 Y. Guo, S. Apergi, N. Li, M. Chen, C. Yin, Z. Yuan, F. Gao, F. Xie, G. Brocks, S. Tao and N. Zhao, *Nat. Commun.*, 2021, **12**, 644.

116 N. Jiang, Z. Wang, Y. Zheng, Q. Guo, W. Niu, R. Zhang, F. Huang and D. Chen, *Nano Energy*, 2022, **97**, 107181.

117 T.-H. Han, J.-W. Lee, Y. J. Choi, C. Choi, S. Tan, S.-J. Lee, Y. Zhao, Y. Huang, D. Kim and Y. Yang, *Adv. Mater.*, 2020, **32**, 1905674.

118 F. Zhang, B. Cai, J. Song, B. Han, B. Zhang and H. Zeng, *Adv. Funct. Mater.*, 2020, **30**, 2001732.

119 Y. Fu, Q. Zhang, D. Zhang, Y. Tang, L. Shu, Y. Zhu and Z. Fan, *Adv. Funct. Mater.*, 2020, **30**, 2002913.

120 Y. Li, J. Roger, I. Allegro, J. C. Fischer, Q. Jin, U. Lemmer, I. A. Howard and U. W. Paetzold, *Adv. Funct. Mater.*, 2022, **32**, 2200772.

121 F. Ye, H. Zhang, P. Wang, W. Li, D. Li, B. Du, D. Liu and T. Wang, *ACS Appl. Mater. Interfaces*, 2019, **11**, 43452–43459.

122 T. Wu, Y. Yang, Y. Zou, Y. Wang, C. Wu, Y. Han, T. Song, Q. Zhang, X. Gao and B. Sun, *Nanoscale*, 2018, **10**, 19322–19329.

123 L. Zhao, Y. Zhou, Z. Shi, Z. Ni, M. Wang, Y. Liu and J. Huang, *Nat. Photonics*, 2023, **17**, 315–323.

124 F. P. García De Arquer, A. Armin, P. Meredith and E. H. Sargent, *Nat. Rev. Mater.*, 2017, **2**, 16100.

125 Y. He, W. Pan, C. Guo, H. Zhang, H. Wei and B. Yang, *Adv. Funct. Mater.*, 2021, **31**, 2104880.

126 Z. Xu, H. Xi, X. Sun, H. Liu, J. Liu, Y. Ba, D. Chen, G. Zhang, C. Zhang, X. Ma and Y. Hao, *Adv. Funct. Mater.*, 2024, **n/a**, 2400817.

127 Z. Zhao, J. Hao, B. Jia, D. Chu, J. Pi, Y. Zhang, S. Zai, Y. Liang, Y. Li, Z. Feng, X. Zheng, M. Wei, L. Zhao, R. Shi, S. F. Liu and Y. Liu, *ACS Energy Lett.*, 2024, **9**, 2758–2766.

128 D. Luo, T. Zou, W. Yang, B. Xiang, X. Yang, Y. Wang, R. Su, L. Zhao, R. Zhu, H. Zhou, T. P. Russell, H. Yu and Z. Lu, *Adv. Funct. Mater.*, 2020, **30**, 2001692.

129 X. Xu, W. Qian, J. Wang, J. Yang, J. Chen, S. Xiao, Y. Ge and S. Yang, *Adv. Sci.*, 2021, **8**, 2102730.

130 R. Ollearo, A. Caiazzo, J. Li, M. Fattori, A. J. J. M. van Breemen, M. M. Wienk, G. H. Gelinck and R. A. J. Janssen, *Adv. Mater.*, 2022, **34**, 2205261.

131 L. Jiang, Z. Li, Q. Dong, X. Rong and G. Dong, *ACS Appl. Mater. Interfaces*, 2023, **15**, 32647–32655.

132 L. Tao, W. Tang, M. Yan, L. Ding, J. Wei, L. Wang, L. Li, L. Li, D. Yang and Y. Fang, *J. Mater. Chem. C*, 2023, **11**, 12392–12399.

133 X. Zhang, L. Li, C. Ji, X. Liu, Q. Li, K. Zhang, Y. Peng, M. Hong and J. Luo, *Natl. Sci. Rev.*, 2021, **8**, nwab044.

134 Z. Xiaoming, L. Tianran, B. Q. C., L. Tianjun, H. Rudolph, C. Guangming, Y. Nan, G. Feng and L. Yueh-Lin, *Science*, 2022, **0**, eabn5679.

135 L. Wang, Q. Zhou, Z. Zhang, W. Li, X. Wang, Q. Tian, X. Yu, T. Sun, J. Wu, B. Zhang and P. Gao, *J. Energy Chem.*, 2022, **64**, 179–189.

136 B. P. Kore, W. Zhang, B. W. Hoogendoorn, M. Safdari and J. M. Gardner, *Commun. Mater.*, 2021, **2**, 100.

137 S. Kumar, L. Houben, K. Rechav and D. Cahen, *Proc. Natl. Acad. Sci.*, 2022, **119**, e2114740119.

138 J. Chakkamalayath, N. Hiott and P. V Kamat, *ACS Energy Lett.*, 2023, **8**, 169–171.

139 G. Szabó and P. V Kamat, *ACS Energy Lett.*, 2024, **9**, 193–200.

140 C. A. R. Perini, E. Rojas-Gatjens, M. Ravello, A. F. C. Mendez, J. Hidalgo, Y. An, S. Kim, B. Lai, R. Li, C. S. Acuña and J. Correa-Baena, *Adv. Mater.*, 2022, 2204726.

141 A. A. Sutanto, R. Szostak, N. Drigo, V. I. E. Queloz, P. E. Marchezi, J. C. Germino, H. C. N. Tolentino, M. K. Nazeeruddin, A. F. Nogueira and G. Grancini, *Nano Lett.*, 2020, **20**, 3992–3998.

142 A. A. Sutanto, N. Drigo, V. I. E. Queloz, I. Garcia-Benito, A. R. Kirmani, L. Richter, P. Schouwink, K. T. Cho, S. Paek, M. K. Nazeeruddin and G. Grancini, *J. Mater. Chem. A*, 2020, **8**, 2343–2348.

143 S. M. Park, M. Wei, J. Xu, H. R. Atapattu, F. T. Eickemeyer, K. Darabi, L. Grater, Y. Yang, C. Liu, S. Teale, B. Chen, H. Chen, T. Wang, L. Zeng, A. Maxwell, Z. Wang, K. R. Rao, Z. Cai, S. M. Zakeeruddin, J. T. Pham, C. M. Risko, A. Amassian, M. G. Kanatzidis, K. R. Graham, M. Grätzel and E. H. Sargent, *Science*, 2023, **381**, 209–215.

144 C. Liu, Y. Yang, K. Rakstys, A. Mahata, M. Franckevicius, E. Mosconi, R. Skackauskaite, B. Ding, K. G. Brooks, O. J. Usiobo, J.-N. Audinot, H. Kanda, S. Driukas, G. Kavaliauskaite, V. Gulbinas, M. Dessimoz, V. Getautis, F. De Angelis, Y. Ding, S. Dai, P. J. Dyson and M. K. Nazeeruddin, *Nat. Commun.*, 2021, **12**, 6394.

145 L. Luo, H. Zeng, Z. Wang, M. Li, S. You, B. Chen, A. Maxwell, Q. An, L. Cui, D. Luo, J. Hu, S. Li, X. Cai, W. Li, L. Li, R. Guo, R. Huang, W. Liang, Z.-H. Lu, L. Mai, Y. Rong, E. H. Sargent and X. Li, *Nat. Energy*, 2023, **8**, 294–303.

146 A. H. Proppe, M. Wei, B. Chen, R. Quintero-Bermudez, S. O. Kelley and E. H. Sargent, *J. Am. Chem. Soc.*, 2019, **141**, 14180–14189.

147 Y. Kang, R. Li, X. Shen, B. Jin, Y. Zhan, A. Wang, B. Li, Y. Song, G. Xiao and Q. Dong, *Nano Energy*, 2024, **120**, 109178.

148 J. Rodríguez-Romero, J. Sanchez-Diaz, C. Echeverría-Arrondo, S. Masi, D. Esparza, E. M. Barea and I. Mora-Seró, *ACS Energy Lett.*, 2020, **5**, 1013–1021.

149 E. Shi, B. Yuan, S. B. Shiring, Y. Gao, Akriti, Y. Guo, C. Su, M. Lai, P. Yang, J. Kong, B. M. Savoie, Y. Yu and L. Dou, *Nature*, 2020, **580**, 614–620.

150 Akriti, E. Shi, S. B. Shiring, J. Yang, C. L. Atencio-Martinez, B. Yuan, X. Hu, Y. Gao, B. P. Finkenauer, A. J. Pistone, Y. Yu, P.

View Article Online
DOI: 10.1039/D4CC02299H

Liao, B. M. Savoie and L. Dou, *Nat. Nanotechnol.*, 2021, **16**, 584–591.

151 Akriti, S. Zhang, Z.-Y. Lin, E. Shi, B. P. Finkenauer, Y. Gao, A. J. Pistone, K. Ma, B. M. Savoie and L. Dou, *Adv. Mater.*, 2021, **33**, 2105183.

152 M. Wang, Z. Shi, C. Fei, Z. J. D. Deng, G. Yang, S. P. Dunfield, D. P. Fenning and J. Huang, *Nat. Energy*, 2023, **8**, 1229–1239.

153 S.-H. Lee, S. Jeong, S. Seo, H. Shin, C. Ma and N.-G. Park, *ACS Energy Lett.*, 2021, 1612–1621.

154 D. Zhenghong, Y. S. K., C. Min, A. Ali, Q. Yue and P. N. P., *Science*, 2021, **372**, 618–622.

155 C. Luo, G. Zheng, F. Gao, X. Wang, C. Zhan, X. Gao and Q. Zhao, *Nat. Photonics*, , DOI:10.1038/s41566-023-01247-4.

156 H. Min, D. Y. Lee, J. Kim, G. Kim, K. S. Lee, J. Kim, M. J. Paik, Y. K. Kim, K. S. Kim, M. G. Kim4, T. J. Shin and S. Il Seok, *Nature*, 2021, **598**, 444–450.

157 C. Ma, F. T. Eickemeyer, S.-H. Lee, D.-H. Kang, S. J. Kwon, M. Grätzel and N.-G. Park, *Science*, 2023, **379**, 173–178.